

---

# Is Your Diffusion Sampler Actually Correct?

## A Sampler-Centric Evaluation of Discrete Diffusion Language Models

---

Luhan Tang<sup>1</sup> Longxuan Yu<sup>1</sup> Shaorong Zhang<sup>1</sup> Greg Ver Steeg<sup>1</sup>

### Abstract

Discrete diffusion language models (dLLMs) provide a fast and flexible alternative to autoregressive models (ARMs) via iterative denoising with parallel updates. However, their evaluation is challenging: existing metrics conflate denoiser approximation error with sampler-induced error from the sampling dynamics, a problem that does not arise for ARMs whose autoregressive sampling exactly reflects the learned probability model. We introduce a sampler-centric oracle framework that replaces learned denoisers with an exact Hidden Markov Model posterior derived from a ground-truth Markov chain, isolating sampler-induced error in a controlled setting. We show that few-step discrete diffusion samplers are not distributionally correct even under an oracle denoiser, with transition-level mismatch that vanishes only as the number of steps approaches the sequence length. Moreover, improvements in negative log-likelihood, generative perplexity, or MAUVE do not imply correct sampling. Code is available at [https://luhantang.github.io/dllm\\_sampler/](https://luhantang.github.io/dllm_sampler/).

### 1. Introduction

Discrete diffusion language models (dLLMs) have emerged as an alternative to autoregressive models (ARMs) (Radford et al., 2019; Grattafiori et al., 2024; Team et al., 2024) for discrete sequence generation. Rather than strict left-to-right factorization, dLLMs generate sequences through iterative denoising, enabling parallel updates across multiple positions (Austin et al., 2021; Campbell et al., 2022; Chang et al., 2022; Sahoo et al., 2024; Arriola et al., 2025). This formulation offers potential advantages in inference efficiency and supports capabilities that are difficult to realize with ARMs, including bidirectional context utilization, iterative revision, and global constraint satisfaction (Ghazvininejad

<sup>1</sup>University of California, Riverside. Correspondence to: Greg Ver Steeg <gregoryv@ucr.edu>.

Preprint. February 24, 2026.

et al., 2019; Nie et al., 2025). Recent dLLMs have demonstrated competitive performance on standard language modeling benchmarks, motivating further investigation into their properties and limitations.

Despite these architectural differences, existing dLLMs are predominantly evaluated using protocols developed for ARMs, assessing the properties of the final generated samples through task-based metrics such as zero-shot accuracy (Brown et al., 2020; Nie et al., 2025), distribution-based metrics such as perplexity (Austin et al., 2021; Lou et al., 2023; Sahoo et al., 2024), and surface-level metrics such as BLEU or  $n$ -gram diversity (Li et al., 2022). These metrics implicitly assume that observed generation error reflects model quality, an assumption justified for ARMs, where exact ancestral sampling introduces no additional error. In ARMs, the training objective directly optimizes the model distribution, and the correctness of the sampler follows by construction.

However, this assumption does not hold for dLLMs. Their sampling procedures involve approximations: parallel decoding assumes conditional independence among masked positions, and finite-step generation discretizes continuous-time dynamics. Such approximations can introduce systematic bias independent of model quality.

This raises a fundamental evaluation problem: standard metrics conflate two distinct sources of error for dLLMs:

- **Model approximation error:** the learned denoiser  $p_\theta(\cdot | x_t)$  deviates from the true posterior due to limited capacity, optimization constraints, or insufficient training.
- **Sampling Dynamics Error:** introduced by the generation procedure itself, such as conditional independence assumptions in parallel decoding or discretization errors from finite time steps.

Evaluation metrics that observe only final outputs conflate model-approximation and sampling errors, making this separation difficult when the denoiser is learned and the ground-truth posterior is unavailable.

To address this, we propose an **oracle evaluation frame-**

**work** that eliminates model approximation error by construction. We define the data distribution as a discrete Markov chain, for which exact posteriors under partial observations can be computed using a Hidden Markov Model (HMM). Replacing learned denoisers with this oracle isolates sampling dynamics as the sole source of distributional deviation, enabling controlled comparison across sampler designs.

Our contributions are as follows:

1. We introduce a **sampler-centric oracle evaluation framework** for discrete diffusion models, which replaces learned denoisers with an exact HMM posterior from a ground-truth Markov chain, enabling isolation of sampler-induced error under controlled and method-consistent settings.
2. We show that **few-step discrete diffusion is not distributionally correct even under an exact oracle denoiser**. Across SEDD, MDLM, LLaDA, and ReMDM, substantial transition-level mismatch persists at small step counts and vanishes only as the number of diffusion steps approaches the sequence length.
3. We show that **surface-level quality and common metrics do not imply correct sampling**: fluent samples can have large transition KL, reduced entropy, and degraded  $n$ -gram diversity. Likelihood-based metrics (NLL, GenPPL) can improve under biased sampling, while MAUVE may remain insensitive to transition-level errors.

## 2. Background and Problem Setup

### 2.1. Discrete Generation and Sampling

We focus on dLLMs, which generate sequences over a finite vocabulary using an iterative forward–reverse process. Although these models differ in their reverse-time denoiser parameterization and sampling mechanisms, SEDD (Lou et al., 2023), MDLM (Sahoo et al., 2024), LLaDA (Nie et al., 2025), and ReMDM (Wang et al., 2025) share a common two-stage forward–reverse generation framework.

Throughout the paper, we use  $t$  to index diffusion steps,  $u \in \{1, \dots, T\}$  to index token positions within a sequence, and  $v \in \mathcal{V}$  to denote vocabulary elements (token values).

**Forward process.** The forward process progressively corrupts a clean sequence  $x_0$  into a noisy state  $z_t$  at time  $t \in [0, S]$ . It is typically modeled as a factorized Markov process where tokens are independently corrupted (e.g., replaced by a mask token):

$$q(z_t | x_0) = \prod_{u=1}^T q(z_t^{(u)} | x_0^{(u)}), \quad (1)$$

where the marginal probability of a token remaining clean decays according to a schedule  $\alpha_t$ . This process is assumed to be fixed and is used solely for training the denoiser.

**Backward process and sampling.** Generation is performed by reversing this corruption. At each step, a denoiser  $p_\theta$  provides an estimate of the conditional distribution of the clean data given the current noisy state  $z_t$ :

$$p_\theta(x_0 | z_t) \approx p(x_0 | z_t). \quad (2)$$

The sampler then uses this prediction to update the sequence state  $z_t \rightarrow z_{t-1}$ . The specific mechanisms differ across methods:

(1) **SEDD** models the backward process as a continuous-time Markov Chain. It parameterizes the transition rates via a concrete score function representing probability ratios:

$$s_\theta(z_t, u, v) \propto \frac{p_t(z_t^{(u)} = v)}{p_t(z_t)}, \quad (3)$$

which drives the stochastic jumps from masks to tokens using  $\tau$ -leaping.

(2) **MDLM** formulates discrete generation via masked diffusion and assumes conditional independence among masked tokens. The denoiser is factorized as

$$p_\theta(x_0 | z_t) = \prod_{u \in \mathcal{M}_t} p_\theta(x_0^{(u)} | z_t), \quad (4)$$

where  $\mathcal{M}_t$  denotes the set of masked positions at diffusion step  $t$ . It enables parallel updates of masked positions during sampling.

(3) **LLaDA** adopts the same factorized denoiser as MDLM in Equation (4), but introduces a confidence-based parallel remasking strategy. At each step, the sampler selects a subset of masked positions to unmask in parallel based on the denoiser’s confidence scores.

(4) **ReMDM** modifies the reverse transition to allow re-masking. The approximate reverse step samples  $z_{t-1}$  from a mixture:

$$z_{t-1}^{(u)} \sim (1 - \sigma_t) \cdot p_\theta(x_0^{(u)} | z_t) + \sigma_t \cdot \delta_{[M]}, \quad (5)$$

where  $\sigma_t$  controls the probability of discarding a generated token, allowing the sampler to undo previous decisions and perform iterative refinement of errors.  $[M]$  denotes the special mask token, and  $\delta_{[M]}$  places all probability mass on re-masking the current position.

**Role of the sampler.** The distinction between the denoiser and the sampler is crucial. The denoiser provides a local conditional distribution  $p_\theta(x_0 | z_t)$ , while the sampler defines the integration path and update rules (e.g., the re-masking rate  $\sigma_t$  or the step size  $\Delta t$ ). These structural choices can introduce what we refer to as *sampling error*, even when the denoiser itself is accurate. We next introduce a controlled framework designed to isolate sampler-induced error.

### 3. Method: A Controlled Framework to Isolate Sampler Error

Applying forward masking to a discrete-time Markov chain leads to a latent-variable model with exact inference under partial observations, enabling an oracle denoiser that isolates sampler-induced error.

#### 3.1. Ground-Truth Markov Chain Prior

**Ground-truth Markov prior.** We consider a ground-truth data distribution  $p_0$  over sequences  $x_{1:T} = (x_1, \dots, x_T) \in \mathcal{V}^T$ , defined as a discrete-time Markov chain:

$$p_0(x_{1:T}) = \pi_0(x_1) \prod_{i=2}^T P(x_i | x_{i-1}), \quad (6)$$

where  $\mathcal{V}$  is a finite vocabulary,  $\pi_0$  denotes the initial distribution, and  $P$  the transition kernel.

**Computational considerations.** To balance expressiveness, ergodicity, and computational tractability (Norris, 1998), we specify a concrete instantiation of the transition kernel by constructing a sparse Markov prior. Specifically, we define an effective transition kernel  $P'$  that retains only the top- $K$  outgoing transitions per state, with  $K \ll V$ , and includes a small teleport component (Page et al., 1999):

$$P'(v | v') = (1-\varepsilon) P_{\text{top-}K}(v | v') + \varepsilon \nu(v), \quad \varepsilon \in (0, 1). \quad (7)$$

This construction reduces the cost of sampling and oracle evaluation from  $\mathcal{O}(V^2)$  to  $\mathcal{O}(V)$  per time step.

Throughout the paper, the Markov chain in Eq. (6) defines the ground-truth data distribution  $p_0$  over clean sequences. The top- $K$  structure (with teleport mixing) in (7) is intrinsic to the definition of  $p_0$  and is not an approximation introduced during inference.

#### 3.2. HMM Posterior Under Partial Observations

The forward masking process applied to a Markov chain induces a Hidden Markov Model (HMM) (Eddy, 1996; Bishop & Nasrabadi, 2006; Murphy, 2012). The clean sequence forms the latent states, while masked tokens correspond to missing observations. Under this formulation, the exact posterior under partial observations can be computed via standard forward-backward smoothing.

In this subsection, we fix a diffusion step  $t$  and view the resulting noisy sequence  $z_t$  as a partially observed sequence  $z_{1:T}$  for HMM inference. For notational convenience within this HMM formulation, we use  $i$  to index sequence positions, instead of  $u$  used elsewhere in the paper.

**Model definition.** We treat the ground-truth Markov chain in Equation (6) as the latent state sequence of an HMM.

Let  $x_{1:T} \in \mathcal{V}^T$  denote the latent clean sequence (ground-truth states), and let  $z_{1:T} \in \mathcal{V} \cup \{\text{MASK}\}$  denote the partially observed sequence, where MASK indicates a missing observation rather than a stochastic emission.

Define the set of revealed positions

$$\mathcal{R} = \{i \in \{1, \dots, T\} : z_i \neq \text{MASK}\}, \quad (8)$$

and the corresponding hard constraints

$$\mathcal{E} = \{x_i = z_i \text{ for all } i \in \mathcal{R}\}. \quad (9)$$

Under these constraints, the posterior distribution over latent state sequences is

$$p(x_{1:T} | \mathcal{E}) \propto \pi_0(x_1) \prod_{i=2}^T P'(x_i | x_{i-1}) \prod_{i=1}^T \phi_i(x_i), \quad (10)$$

where the emission factors encode hard evidence,

$$\phi_i(v) = \begin{cases} \mathbf{1}\{v = z_i\}, & i \in \mathcal{R}, \\ 1, & i \notin \mathcal{R}. \end{cases} \quad (11)$$

**Forward-backward inference.** To compute posterior marginals efficiently, we apply the standard forward-backward algorithm. Define the forward message

$$\alpha_i(v) := p(x_i = v, \mathcal{E}_{1:i}),$$

and the backward message

$$\beta_i(v) := p(\mathcal{E}_{i+1:T} | x_i = v),$$

where  $\mathcal{E}_{1:i}$  denotes the constraints up to position  $i$ .

The forward recursion is given by

$$\alpha_i(v) = \phi_i(v) \sum_{v' \in \mathcal{V}} \alpha_{i-1}(v') P'(v | v'), \quad (12a)$$

$$\alpha_1(v) = \pi_0(v) \phi_1(v), \quad (12b)$$

where we choose the initial distribution  $\pi_0$  to be the stationary distribution of  $P'$ .

The backward recursion is given by

$$\beta_i(v) = \sum_{v' \in \mathcal{V}} P'(v' | v) \phi_{i+1}(v') \beta_{i+1}(v'), \quad \beta_T(v) = 1. \quad (13)$$

**Oracle denoiser.** The marginal posterior at position  $i$  is

$$\gamma_i(v) := p^*(x_i = v | z_{1:T}) = \frac{\alpha_i(v) \beta_i(v)}{\sum_{v'' \in \mathcal{V}} \alpha_i(v'') \beta_i(v'')}. \quad (14)$$

Here  $p^*(x_i | z_{1:T})$  denotes the *ground-truth oracle posterior marginal* at position  $i$ , uniquely induced by the known

Markov transition kernel  $P'$  and the hard evidence  $z_{1:T}$  via exact HMM smoothing. The quantity  $\gamma_i$  is its *explicit representation* computed by the forward–backward algorithm.

We use  $\gamma_i$  as an oracle denoiser, representing the exact conditional distribution of a clean token given the partially observed sequence. Its derivation via the forward–backward algorithm and log-domain numerical details are provided in Appendices A.

**Interpretation.** Equation (10) corresponds to HMM smoothing under masking observations and is independent of the specific noising process.

## 4. Oracle Instantiations for Discrete Samplers

To decouple sampling error from approximation error, we systematically replace the learned denoiser in several representative discrete samplers with an exact oracle posterior  $p^*$ , defined by the ground-truth Markov chain and computed via exact HMM smoothing (Section 3.2), which is held fixed throughout. What differs across samplers is how this same oracle posterior, represented by its marginal  $\gamma_{t,u}$ , is used to drive the sampling dynamics.

Given a diffusion state  $z_t$ , we interpret the masked sequence  $z_t \in \mathcal{V}^T \cup \{[\text{MASK}]\}$  as a partially observed sequence for HMM inference. We detail the resulting oracle-driven instantiations for SEDD, MDLM, LLaDA, and ReMDM below. See Appendix C for full oracle-instantiation details for each sampler.

### 4.1. SEDD: Oracle Scores and Calibration Analysis

SEDD (Lou et al., 2023) operates on concrete scores rather than direct token probabilities. To enable exact oracle-driven sampling, we derive the required scores from the oracle posterior.

**Oracle score derivation.** For a masked position  $u$  and candidate token  $v$ , the exact score required by the  $\tau$ -leaping solver is given by

$$s^*(z_t, u, v) \propto \gamma_{t,u}(v), \quad (15)$$

where  $\gamma_{t,u}(v)$  denotes the oracle marginal probability of token  $v$  at position  $u$  given the noisy sequence  $z_t$  at diffusion step  $t$ , as computed via forward–backward in Eq. (14). The full derivation, including the noise schedule terms, is provided in Appendix B.

**Sensitivity analysis: temperature-induced score sharpening.**

Recent work shows that low-precision Gumbel-based categorical sampling can implicitly induce low-temperature behavior, leading to over-confident token distributions (Zheng et al., 2024). Motivated by this observation, we simulate

controlled score overconfidence by applying temperature scaling to the oracle score:

$$\log s^{(\beta)}(z_t, u, v) \propto \beta \cdot \log \gamma_{t,u}(v), \quad (16)$$

where  $\beta = 1$  recovers the exact oracle and  $\beta > 1$  sharpens the distribution while preserving token rankings. Any resulting degradation therefore reflects sampler sensitivity to score miscalibration rather than denoiser error.

### 4.2. MDLM & LLaDA: Oracle Marginals and Parallel Decoding

MDLMs (Sahoo et al., 2024) and LLaDA (Nie et al., 2025) perform non-autoregressive decoding by updating multiple masked positions in parallel. In our oracle evaluation, we replace the learned denoiser with exact oracle marginals,

$$p_\theta(x_0 | z_t) \mapsto \prod_{u=1}^T \gamma_{t,u}(\cdot), \quad (17)$$

which implicitly assumes conditional independence across positions.

**MDLM.** With the factorized oracle marginals, MDLM-style samplers update masked positions in parallel using simple unmasking schedules (e.g., random or uniform selection), making the effects of the independence approximation explicit.

**LLaDA.** LLaDA uses the same factorized oracle marginals but applies a confidence-based parallel remasking strategy to select positions at each step. Comparisons to the autoregressive baseline therefore isolate the cost of this non-autoregressive decoding.

### 4.3. ReMDM: Oracle-Guided Re-masking

ReMDM (Wang et al., 2025) extends masked diffusion by allowing tokens to be re-masked and re-sampled during generation, enabling iterative refinement.

**Evaluated variants.** We evaluate two oracle-driven ReMDM variants that differ in their re-masking schedules.

- **Oracle-ReMDM-conf.** Uses confidence-based re-masking. In the oracle setting, the confidence at position  $u$  is defined as

$$\text{Conf}(u) = \gamma_{t,u}(c_t^{(u)}),$$

and tokens with lower oracle confidence are re-masked more frequently. We use *ReMDM* and *ReMDM-conf* interchangeably to refer to this variant.

- **Oracle-ReMDM-loop.** Uses a loop-based re-masking schedule, where re-masking is active only within a

diffusion-time window  $t_{\text{off}} < t \leq t_{\text{on}}$ . Outside this window, the sampler reduces to standard MDLM updates. Within the loop window, re-masking follows a capped schedule

$$\sigma_t = \min\{\eta_{\text{cap}}, \sigma_t^{\text{max}}\},$$

where  $\eta_{\text{cap}}$  is a fixed cap on the re-masking probability, and  $\sigma_t^{\text{max}}$  ensures valid posterior probabilities.

**Nucleus sampling.** Following Holtzman et al. (2019) and the original ReMDM implementation, we optionally apply nucleus (top- $p$ ) sampling. We evaluate both ReMDM variants with and without nucleus sampling to isolate the effect of re-masking under a fixed oracle denoiser.

**Summary and positioning.** Across all oracle instantiations, the oracle posterior is used in a method-consistent manner, without altering the original sampling logic. Nucleus (top- $p$ ) sampling in ReMDM is inherited from the original method as a decoding mechanism, whereas temperature scaling in SEDD is an intentionally introduced perturbation used to probe sampler sensitivity.

## 5. Metrics

All distributional metrics are derived from empirical statistics over token-to-token transitions under the oracle kernel, rather than from marginal token frequencies.

We organize our evaluation metrics into the following categories; complete definitions are provided in Appendix D.

**Transition-level correctness.** Our primary metrics measure agreement between the empirical transition distribution  $\hat{p}(x_{t+1} | x_t)$  and the oracle transition kernel  $P'$ .

We report sequence negative log-likelihood (per token), abbreviated as Sequence NLL (per token), the full transition KL rate (Transition KL), and the transition entropy rate (Transition Entropy). Lower transition NLL and KL indicate closer agreement with the ground-truth transition kernel, while entropy helps diagnose over-sharpening or excessive randomness.

**Sequence-level diversity.** We report simple sequence-level statistics to characterize surface diversity. These include the Duplication rate and  $n$ -gram diversity ratios (2/3-gram). Such metrics do not measure distributional correctness, but provide useful context for qualitative generation behavior.

**Coverage and collapse.** We additionally track coverage-related diagnostics, including the fraction of transitions outside the top- $K$  support and the effective support size. Here, the support refers to the set of token transitions with non-negligible probability under the oracle transition distribution.

**External language-model metrics.** We report generative perplexity (GenPPL) and MAUVE using a pretrained GPT-2 Large model as the evaluator, where lower GenPPL and higher MAUVE are conventionally interpreted as better. We treat both as auxiliary diagnostics rather than primary correctness metrics.

## 6. Experimental Setup

Across all experiments, we fix the sequence length  $T = 1024$ , sample  $N = 512$  sequences per setting, and vary the number of diffusion steps  $S \in \{8, 16, 32, 64, 128, 256, 512, 1024\}$ .

**Data and Oracle Construction.** We primarily evaluate sampler behavior on OpenWebText (OWT) at the token level (Gokaslan et al., 2019), which serves as our main evaluation dataset. We tokenize OWT using a ByteBPE vocabulary of size  $V = 4096$  for computational tractability. On the resulting token sequences, we construct a bigram transition model and sparsify it via top- $K$  truncation, preserving at least 99% cumulative transition mass per state. The global sparsity level  $K$  is chosen as the 90th percentile of the per-state effective supports, yielding  $K = 206$ . We additionally apply a small fixed teleport probability  $\varepsilon = 10^{-4}$ . For completeness, we report supplementary experiments on Text8 at the character level (Sukhbaatar et al., 2015), which uses a dense bigram prior. Full dataset, tokenizer, and oracle construction details are provided in Appendix E.

**Controlled sampler perturbations.** All samplers are evaluated under a shared oracle posterior across varying diffusion step counts. For SEDD, we apply temperature scaling to the oracle score, with  $\beta = 1$  corresponding to exact sampling and  $\beta > 1$  inducing low-temperature sharpening, and evaluate a range of  $\beta$  values. For ReMDM, we compare loop-based and confidence-based re-masking schedules, each with and without nucleus (top- $p$ ) sampling ( $p = 0.9$ ). Inference-time scaling follows Wang et al. (2025) using the max-capped schedule with  $\eta_{\text{cap}} = 0.02$ . For the loop-based variant, we use  $t_{\text{on}} = 0.55$ ,  $t_{\text{off}} = 0.05$ , and  $\alpha(t_{\text{on}}) = 0.9$ .

## 7. Experimental Results and Analysis

We report and analyze results on sampler-induced error under an oracle denoiser, the behavior of common evaluation metrics, and the impact of different sampler designs.

### 7.1. Sampler-induced error does not vanish in the few-step regime

Figure 1 shows that, on OpenWebText under an exact oracle denoiser, all discrete diffusion samplers exhibit substantial transition-level error at small numbers of sampling steps.

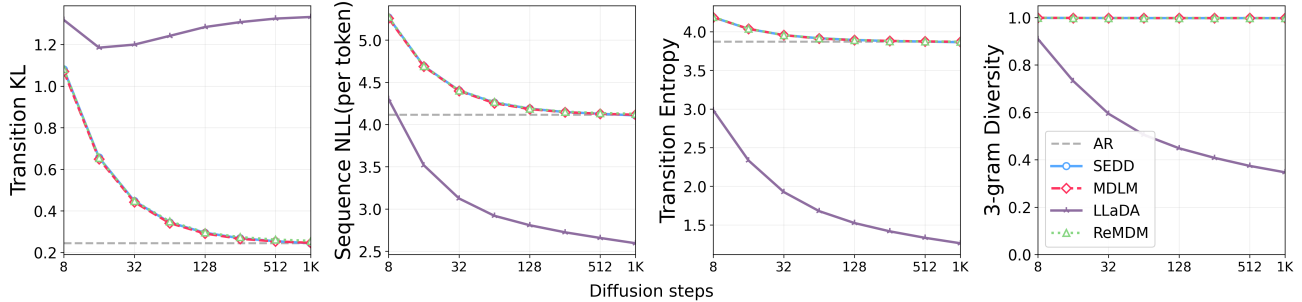


**Figure 1. Transition-level metrics on OpenWebText (OWT) under an oracle denoiser.** We report transition KL, NLL, entropy rate, and  $n$ -gram diversity as functions of the number of sampling steps for several discrete diffusion samplers, using an exact oracle posterior to isolate sampler-induced error. For all samplers, substantial transition-level error persists at small step counts, with convergence to the autoregressive baseline occurring only when the number of steps approaches the sequence length  $T$  (except LLaDA). Notably, LLaDA attains very low sequence NLL at few steps, despite severe degradation in transition KL, entropy, and diversity, demonstrating that NLL alone is not a reliable indicator of distributional correctness. All samplers show zero exact duplication.

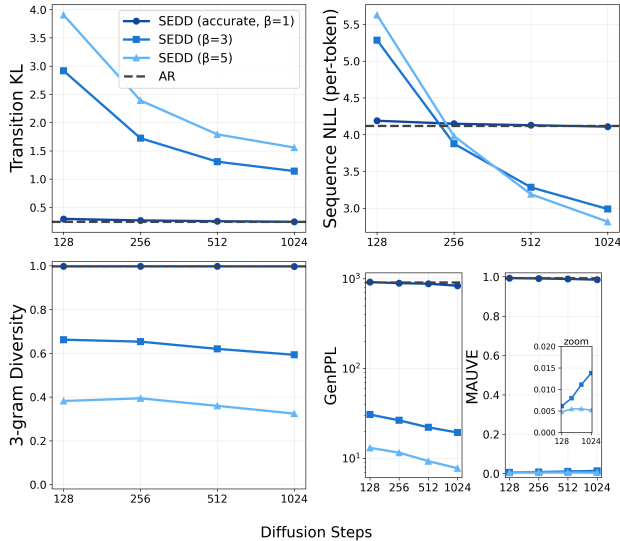


**Figure 2. Temperature-induced score sharpening in SEDD under an oracle denoiser (OWT).** As  $\beta$  increases, transition KL rises and 3-gram diversity falls, while sequence NLL and GenPPL decrease. MAUVE drops sharply at low temperatures, indicating severe distributional degradation. This reveals a misalignment between likelihood-based metrics and transition-level correctness. Duplication remains negligible except under extreme sharpening (Appendix F.2).

Across transition KL, NLL, and entropy, convergence to the autoregressive baseline occurs only when the number of steps approaches the sequence length  $T$  (except for LLaDA). The same qualitative behavior holds on the character-level Text8 dataset despite the different vocabulary and granularity; see Figure 6 in Appendix F.2.

**Interpretation.** This behavior reflects a structural limitation of few-step discrete diffusion. Sampling proceeds via parallel updates of marginal token distributions. Matching marginals implies matching the joint distribution only un-

der strong independence assumptions, which are violated in natural language. Consequently, transition-level inconsistencies persist unless the number of steps approaches the sequence length  $T$ , where the procedure degenerates to autoregressive generation. In short, few-step dLLMs do not converge to the true transition law even with an exact oracle denoiser. See Appendix F.1 for all metric outputs.

## 7.2. Effect of temperature scaling

Figure 2 shows that increasing the sharpening factor  $\beta$  ( $\beta > 1$ ) substantially increases transition KL and reduces 3-gram diversity, indicating growing deviation from the true transition distribution. In contrast, sequence NLL and GenPPL decrease monotonically with  $\beta$ , suggesting apparent improvement under low-temperature sampling. At the same time, MAUVE drops sharply, revealing severe degradation in distributional similarity.

**Interpretation.** Temperature scaling concentrates probability mass on fewer high-density patterns. This locally improves likelihood-based metrics such as NLL and GenPPL, while distorting the true transition law, as reflected by higher KL and reduced diversity. The sharp decline in MAUVE highlights its sensitivity to low-temperature collapse. Overall, these results show that GenPPL can misleadingly improve under distributional distortion, whereas MAUVE more faithfully detects low-temperature degradation.

## 7.3. Generative Perplexity Can Be Misleading

To isolate the behavior observed under temperature scaling in SEDD, we conduct a minimal sanity check using a simple autoregressive bigram model. As shown in Figure 3, local sharpening monotonically reduces GenPPL, reaching values as low as 1.27, while simultaneously collapsing  $n$ -gram diversity and sentence entropy. In fact, GenPPL drops from 688.4 under accurate sampling ( $\beta = 1$ ) to 1.27 at  $\beta = 25$ , a

reduction of more than two orders of magnitude.

This behavior closely mirrors the trends observed in SEDD, despite the absence of diffusion dynamics or learned denoising. Notably, several recent works report state-of-the-art sampling performance based primarily on GenPPL values substantially higher than this.

These results demonstrate that GenPPL can be systematically improved through local sharpening alone, without faithful sampling of the underlying data distribution, and should therefore be interpreted as an evaluator-alignment metric rather than a reliable indicator of sampler correctness.

#### 7.4. Step-wise Evaluation of Oracle ReMDM Variants

Figure 4 shows the interaction between ReMDM re-masking schedules, nucleus sampling, MAUVE, and transition-level metrics.

**Nucleus sampling and transition-level behavior.** Applying nucleus (top- $p$ ) sampling makes sampled token-to-token transitions closer to the oracle transition distribution, reducing transition KL, NLL, and entropy by suppressing low-probability tail transitions. This comes at the cost of a reduced support fraction due to truncation of low-probability transitions.

Across diffusion steps, ReMDM-conf remains consistently closer to the oracle transition kernel, while ReMDM-loop exhibits substantially larger transition-level error across KL, entropy, and support statistics.

**MAUVE behavior across steps.** Despite these pronounced changes in transition KL as the number of diffusion steps increases, MAUVE scores remain uniformly high and vary only weakly, including in the few-step regime where KL changes substantially. This indicates limited sensitivity of MAUVE to transition-level error.

Prior work (Wang et al., 2025) reports that at very large diffusion steps (e.g., 1024 and 4096), ReMDM-loop attains higher MAUVE than ReMDM-conf, and that nucleus sampling further increases MAUVE. In our experiments (up to 1024 steps), we observe only marginal differences: loop and nucleus variants achieve slightly higher MAUVE, but the variation across steps remains small. Under oracle evaluation, ReMDM-loop exhibits substantially larger transition-level error than ReMDM-conf. This reveals a mismatch between surface-level distributional similarity and transition-level correctness.

Taken together, these results suggest that while MAUVE can reflect heuristic-induced support modifications (e.g., nucleus), it may remain largely insensitive to transition-level deviations that do not substantially alter the global sample distribution.

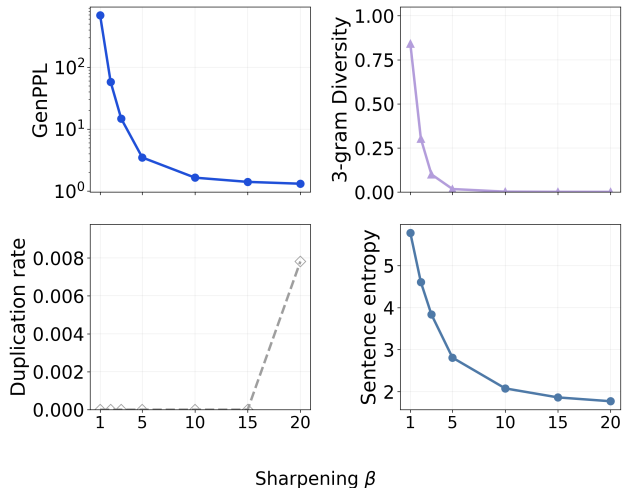


Figure 3. **GenPPL under controlled local sharpening in an autoregressive bigram generator (OWT).** We introduce a sharpening factor  $\beta$  ( $\beta = 1$  corresponds to accurate sampling) and evaluate fixed samples using a pretrained GPT-2 Large model. As  $\beta$  increases, GenPPL decreases monotonically, while 3-gram diversity collapses and sentence entropy steadily declines, indicating increasing concentration of probability mass. Exact duplication remains negligible until extreme sharpening.

#### 7.5. Sampler-induced error in LLaDA

LLaDA presents an instructive failure mode (Figure 1) in which transition NLL appears close to the autoregressive baseline at small step counts, yet the sampler does not converge in transition KL, entropy, or  $n$ -gram diversity.

Under unconditional generation, LLaDA exhibits clear sampler-induced degeneration that intensifies with more diffusion steps: samples become increasingly template-driven and repetitive (e.g., repeated phrases such as “the same time . . . the same time . . .”), despite the absence of exact duplication (Appendix Table 4). For comparison, we also report ground-truth samples and ReMDM generations under identical settings, highlighting that this degeneration is specific to LLaDA’s sampling mechanism rather than an artifact of the oracle chain itself (Appendix Table 3). We also evaluate LLaDA under a minimal conditional setting with a one-token prompt and observe qualitatively indistinguishable behavior, due to rapid HMM mixing under the first-order Markov oracle prior (Appendix Figure 9).

This behavior reflects a strong coupling between LLaDA’s sampling mechanism and its learned denoiser. The sampler relies on denoiser-produced confidence scores that encode rich linguistic priors, effectively shaping the re-masking dynamics. When the denoiser is replaced by an oracle posterior that does not share these priors, this coupling breaks down, causing probability mass to concentrate on a small set of high-frequency transition patterns as sampling steps increase.

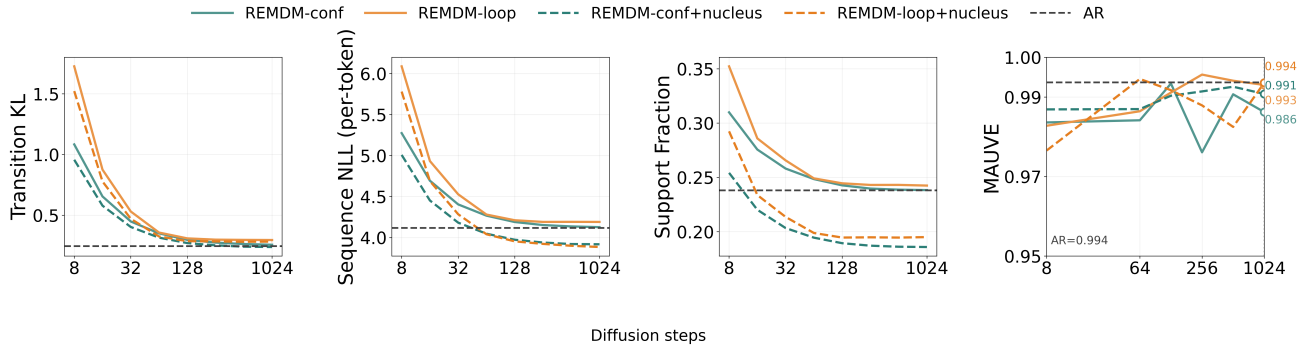


Figure 4. **Step-wise evaluation of oracle ReMDM variants on OWT.** Across transition-level metrics, the ReMDM-loop sampler exhibits larger deviations from the AR baseline than ReMDM-conf, indicating higher sampler error, while ReMDM-conf remains consistently closer to the oracle transition kernel. Applying nucleus sampling reduces transition KL, NLL, and entropy, indicating improved alignment with the oracle kernel, but decreases the support fraction due to truncation of low-probability tail transitions. External MAUVE scores remain high and vary only mildly across diffusion steps. A full breakdown of all reported metrics is provided in Appendix Figure 8.

Such concentration is not inherently undesirable for all applications. Many NLP tasks, such as math problem solving or factual generation, may benefit from reduced diversity, and LLaDA is primarily evaluated using task-level or conditional metrics that emphasize accuracy over coverage.

However, different downstream applications place different requirements on diversity. While reduced diversity can be beneficial for exact-answer tasks, domains such as protein design rely critically on broad coverage to explore viable solutions (Watson et al., 2022). Our results show that, when evaluated as a generative process under an oracle posterior, LLaDA exhibits substantial sampler-induced error as systematic concentration. Distinguishing downstream task utility from sampler correctness is therefore essential.

## 8. Related Work

**Discrete diffusion language models.** Discrete diffusion language models (dLLMs) enable parallel token updates and provide a non-autoregressive alternative to language modeling (Austin et al., 2021; Li et al., 2022; Lou et al., 2023) and more recently (Sahoo et al., 2024; Chen et al., 2025; Wang et al., 2025). While these models allow efficient parallel decoding, their sampling procedures introduce additional sources of approximation beyond model training. Recent work has begun to investigate sampling error in dLLMs (Zheng et al., 2024; Park et al., 2025; Liang et al., 2025; Peng et al., 2025; Zhao et al., 2025; Kang et al., 2025; Chen et al., 2025), typically evaluating degradation through final generated samples. In such settings, sampler error remains entangled with model approximation error.

**Parallel decoding and independence assumptions.** Several works attribute quality degradation to independence assumptions in parallel updates. Chen et al. (2025) analyze parallel unmasking under oracle conditionals and derive

error bounds based on idealized assumptions. Kang et al. (2025) empirically show that ignoring token dependence leads to noticeable quality drops. These studies highlight structural limitations of parallel decoding, but do not disentangle sampler-induced error from imperfections in the learned denoiser.

**Evaluation metrics for diffusion language models.** Another line of work questions the reliability of evaluation metrics for diffusion models. Zheng et al. (2024) show that conclusions can depend strongly on metric choice, and that likelihood-based metrics such as GenPPL may be misleading. Similar observations appear in ReMDM (Wang et al., 2025), where improvements in GenPPL do not consistently translate to downstream quality. However, because these studies evaluate full models, they cannot determine whether such discrepancies arise from model error or from the sampling procedure itself.

**Optimal denoisers and inference hardness.** Recent theoretical work analyzes sampling in diffusion, flow-based, and autoregressive models from a statistical physics perspective (Ghio et al., 2024), characterizing optimal denoisers and the hardness of inference in complex graphical models. These analyses show that computing the optimal posterior or score via message passing can become intractable in loopy or high-complexity regimes. Complementary work studies settings in which exact score models can be constructed under specific structural assumptions (Albrychiewicz et al., 2026). While these studies examine the existence and tractability of optimal denoisers, they do not investigate the empirical behavior of sampling algorithms when the denoiser is exact.

## 9. Conclusion

We introduced an oracle-based evaluation framework that isolates sampler-induced error in discrete diffusion language

models by replacing learned denoisers with an exact ground-truth posterior. This controlled setting allows us to disentangle sampling dynamics from model approximation and directly assess distributional correctness. Our experiments show that few-step diffusion samplers remain substantially biased even under oracle denoising, with transition-level mismatch diminishing only as the number of sampling steps approaches the sequence length.

We further find that commonly used surface-level metrics do not reliably reflect this behavior. In particular, GenPPL can be systematically improved through local sharpening without faithful sampling of the underlying distribution, while MAUVE is highly sensitive to extreme global collapse but often remains insensitive to substantial transition-level deviations across diffusion steps. These findings highlight the need for transition-aware and multi-dimensional evaluation rather than reliance on a single aggregated metric.

## Impact Statement

This paper presents work whose goal is to advance the field of machine learning by improving the understanding and evaluation of discrete diffusion-based sequence samplers. The contributions are methodological and experimental in nature. We do not foresee any specific ethical concerns or broader societal risks arising from this work.

## References

- Albrychiewicz, E., Valiente, A. F., and Chen, L.-C. Dynamical regimes of multimodal diffusion models. *arXiv preprint arXiv:2602.04780*, 2026.
- Arriola, M., Gokaslan, A., Chiu, J. T., Yang, Z., Qi, Z., Han, J., Sahoo, S. S., and Kuleshov, V. Block diffusion: Interpolating between autoregressive and diffusion language models. *arXiv preprint arXiv:2503.09573*, 2025.
- Austin, J., Johnson, D. D., Ho, J., Tarlow, D., and Van Den Berg, R. Structured denoising diffusion models in discrete state-spaces. *Advances in neural information processing systems*, 34:17981–17993, 2021.
- Bishop, C. M. and Nasrabadi, N. M. *Pattern recognition and machine learning*, volume 4. Springer, 2006.
- Brown, T., Mann, B., Ryder, N., Subbiah, M., Kaplan, J. D., Dhariwal, P., Neelakantan, A., Shyam, P., Sastry, G., Askell, A., et al. Language models are few-shot learners. *Advances in neural information processing systems*, 33:1877–1901, 2020.
- Campbell, A., Benton, J., De Bortoli, V., Rainforth, T., Deligiannidis, G., and Doucet, A. A continuous time framework for discrete denoising models. *Advances in Neural Information Processing Systems*, 35:28266–28279, 2022.
- Chang, H., Zhang, H., Jiang, L., Liu, C., and Freeman, W. T. Maskgit: Masked generative image transformer. In *Proceedings of the IEEE/CVF conference on computer vision and pattern recognition*, pp. 11315–11325, 2022.
- Chen, S., Cong, K., and Li, J. Optimal inference schedules for masked diffusion models. *arXiv preprint arXiv:2511.04647*, 2025.
- Eddy, S. R. Hidden markov models. *Current opinion in structural biology*, 6(3):361–365, 1996.
- Ghazvininejad, M., Levy, O., Liu, Y., and Zettlemoyer, L. Mask-predict: Parallel decoding of conditional masked language models. *arXiv preprint arXiv:1904.09324*, 2019.
- Ghio, D., Dandi, Y., Krzakala, F., and Zdeborová, L. Sampling with flows, diffusion, and autoregressive neural networks from a spin-glass perspective. *Proceedings of the National Academy of Sciences*, 121(27):e2311810121, 2024.
- Gokaslan, A., Cohen, V., Pavlick, E., and Tellex, S. Openwebtext corpus, 2019.
- Grattafiori, A., Dubey, A., Jauhri, A., Pandey, A., Kadian, A., Al-Dahle, A., Letman, A., Mathur, A., Schelten, A., Vaughan, A., et al. The llama 3 herd of models. *arXiv preprint arXiv:2407.21783*, 2024.
- Holtzman, A., Buys, J., Du, L., Forbes, M., and Choi, Y. The curious case of neural text degeneration. *arXiv preprint arXiv:1904.09751*, 2019.
- Kang, W., Galim, K., Oh, S., Lee, M., Zeng, Y., Zhang, S., Hooper, C., Hu, Y., Koo, H. I., Cho, N. I., et al. Parallel-bench: Understanding the trade-offs of parallel decoding in diffusion llms. *arXiv preprint arXiv:2510.04767*, 2025.
- Li, X., Thickstun, J., Gulrajani, I., Liang, P. S., and Hashimoto, T. B. Diffusion-lm improves controllable text generation. *Advances in neural information processing systems*, 35:4328–4343, 2022.
- Liang, Y., Liang, Y., Lai, L., and Shroff, N. Discrete diffusion models: Novel analysis and new sampler guarantees. *arXiv preprint arXiv:2509.16756*, 2025.
- Lou, A., Meng, C., and Ermon, S. Discrete diffusion modeling by estimating the ratios of the data distribution. *arXiv preprint arXiv:2310.16834*, 2023.
- Murphy, K. P. *Machine learning: a probabilistic perspective*. MIT press, 2012.
- Nie, S., Zhu, F., You, Z., Zhang, X., Ou, J., Hu, J., Zhou, J., Lin, Y., Wen, J.-R., and Li, C. Large language diffusion models. *arXiv preprint arXiv:2502.09992*, 2025.

- Norris, J. R. *Markov chains*. Number 2. Cambridge university press, 1998.
- Page, L., Brin, S., Motwani, R., and Winograd, T. The pagerank citation ranking: Bringing order to the web. Technical report, Stanford infolab, 1999.
- Park, Y.-H., Lai, C.-H., Hayakawa, S., Takida, Y., and Mitsufuji, Y. Jump your steps: Optimizing sampling schedule of discrete diffusion models. In *The Thirteenth International Conference on Learning Representations*, 2025. URL <https://openreview.net/forum?id=pD6TiCpyDR>.
- Peng, F. Z., Bezemek, Z., Patel, S., Rector-Brooks, J., Yao, S., Bose, A. J., Tong, A., and Chatterjee, P. Path planning for masked diffusion model sampling. *arXiv preprint arXiv:2502.03540*, 2025.
- Pillutla, K., Swayamdipta, S., Zellers, R., Thickstun, J., Welleck, S., Choi, Y., and Harchaoui, Z. Mauve: Measuring the gap between neural text and human text using divergence frontiers. *Advances in Neural Information Processing Systems*, 34:4816–4828, 2021.
- Radford, A., Wu, J., Child, R., Luan, D., Amodei, D., Sutskever, I., et al. Language models are unsupervised multitask learners. *OpenAI blog*, 1(8):9, 2019.
- Sahoo, S., Arriola, M., Schiff, Y., Gokaslan, A., Marroquin, E., Chiu, J., Rush, A., and Kuleshov, V. Simple and effective masked diffusion language models. *Advances in Neural Information Processing Systems*, 37:130136–130184, 2024.
- Sukhbaatar, S., Weston, J., Fergus, R., et al. End-to-end memory networks. *Advances in neural information processing systems*, 28, 2015.
- Team, G., Georgiev, P., Lei, V. I., Burnell, R., Bai, L., Gulati, A., Tanzer, G., Vincent, D., Pan, Z., Wang, S., et al. Gemini 1.5: Unlocking multimodal understanding across millions of tokens of context. *arXiv preprint arXiv:2403.05530*, 2024.
- Wang, G., Schiff, Y., Sahoo, S. S., and Kuleshov, V. Re-masking discrete diffusion models with inference-time scaling. *arXiv preprint arXiv:2503.00307*, 2025.
- Watson, J. L., Juergens, D., Bennett, N. R., Trippe, B. L., Yim, J., Eisenach, H. E., Ahern, W., Borst, A. J., Ragotte, R. J., Milles, L. F., et al. Broadly applicable and accurate protein design by integrating structure prediction networks and diffusion generative models. *BioRxiv*, pp. 2022–12, 2022.
- Zhao, Y., Shi, J., Chen, F., Druckmann, S., Mackey, L., and Linderman, S. Informed correctors for discrete diffusion models. In *The Thirty-ninth Annual Conference on Neural Information Processing Systems*, 2025. URL <https://openreview.net/forum?id=HDeIb67lJe>.
- Zheng, K., Chen, Y., Mao, H., Liu, M.-Y., Zhu, J., and Zhang, Q. Masked diffusion models are secretly time-agnostic masked models and exploit inaccurate categorical sampling. *arXiv preprint arXiv:2409.02908*, 2024.

## A. Derivation of the Oracle Posterior via Forward–Backward

This appendix provides a detailed derivation of the oracle posterior  $p(x_i \mid \mathcal{E})$  for a discrete Markov-chain ground-truth model under partial (hard-evidence) observations. We review the standard forward–backward algorithm for hidden Markov models, derive the forward and backward recursions explicitly, and then specialize the result to deterministic masking observations and to the rank-1 teleport transition used in our experiments. We conclude with a numerically stable log-domain implementation.

### A.1. Hidden Markov Model Setup

Let  $x_{1:T} = (x_1, \dots, x_T) \in \mathcal{V}^T$  denote a discrete-time Markov chain with initial distribution  $\pi_0$  and transition kernel  $P'$ ,

$$p_0(x_{1:T}) = \pi_0(x_1) \prod_{i=2}^T P'(x_i \mid x_{i-1}). \quad (18)$$

We consider partial observations  $z_{1:T} \in \mathcal{V} \cup \{\text{MASK}\}$ , where MASK denotes a missing observation rather than a stochastic emission. This induces a hidden Markov model (HMM) in which  $x_i$  are latent states and  $z_i$  provide hard evidence at revealed positions.

Let

$$\mathcal{R} := \{i : z_i \neq \text{MASK}\}, \quad \mathcal{E} := \{x_i = z_i, \forall i \in \mathcal{R}\}.$$

The inference task of interest is the smoothing posterior

$$p(x_i = v \mid \mathcal{E}), \quad i = 1, \dots, T. \quad (19)$$

### A.2. Forward Recursion (Derivation)

Define the forward message

$$\alpha_i(v) := p(z_{1:i}, x_i = v), \quad v \in \mathcal{V}. \quad (20)$$

By the law of total probability,

$$\alpha_i(v) = \sum_{v' \in \mathcal{V}} p(z_{1:i}, x_{i-1} = v', x_i = v). \quad (21)$$

Applying the chain rule,

$$p(z_{1:i}, x_{i-1} = v', x_i = v) = p(z_i \mid z_{1:i-1}, x_{i-1} = v', x_i = v) p(z_{1:i-1}, x_{i-1} = v', x_i = v). \quad (22)$$

By the HMM conditional independence structure,  $z_i \perp (x_{i-1}, z_{1:i-1}) \mid x_i$ , so

$$p(z_i \mid z_{1:i-1}, x_{i-1} = v', x_i = v) = p(z_i \mid x_i = v).$$

Applying the chain rule again,

$$p(z_{1:i-1}, x_{i-1} = v', x_i = v) = p(x_i = v \mid z_{1:i-1}, x_{i-1} = v') p(z_{1:i-1}, x_{i-1} = v'). \quad (23)$$

By the Markov property,  $x_i \perp z_{1:i-1} \mid x_{i-1}$ , hence

$$p(x_i = v \mid z_{1:i-1}, x_{i-1} = v') = p(x_i = v \mid x_{i-1} = v').$$

Substituting these relations and identifying  $p(z_{1:i-1}, x_{i-1} = v') = \alpha_{i-1}(v')$  yields the forward recursion

$$\alpha_i(v) = p(z_i \mid x_i = v) \sum_{v' \in \mathcal{V}} \alpha_{i-1}(v') P'(v \mid v'). \quad (24)$$

The initialization is  $\alpha_1(v) = \pi_0(v) p(z_1 \mid x_1 = v)$ .

### A.3. Backward Recursion (Derivation)

Define the backward message

$$\beta_i(v) := p(z_{i+1:T} \mid x_i = v), \quad v \in \mathcal{V}. \quad (25)$$

By marginalizing over  $x_{i+1}$ ,

$$\beta_i(v) = \sum_{v' \in \mathcal{V}} p(z_{i+1:T}, x_{i+1} = v' \mid x_i = v). \quad (26)$$

Applying the chain rule,

$$p(z_{i+1:T}, x_{i+1} = v' \mid x_i = v) = p(z_{i+1:T} \mid x_{i+1} = v', x_i = v) p(x_{i+1} = v' \mid x_i = v). \quad (27)$$

By the HMM graphical structure,  $z_{i+1:T} \perp x_i \mid x_{i+1}$ , so

$$p(z_{i+1:T} \mid x_{i+1} = v', x_i = v) = p(z_{i+1:T} \mid x_{i+1} = v').$$

Factoring the future observations,

$$p(z_{i+1:T} \mid x_{i+1} = v') = p(z_{i+1} \mid x_{i+1} = v') p(z_{i+2:T} \mid x_{i+1} = v'), \quad (28)$$

and recognizing  $p(z_{i+2:T} \mid x_{i+1} = v') = \beta_{i+1}(v')$ , we obtain

$$\beta_i(v) = \sum_{v' \in \mathcal{V}} p(z_{i+1} \mid x_{i+1} = v') P'(v' \mid v) \beta_{i+1}(v'). \quad (29)$$

The terminal condition is  $\beta_T(v) = 1$ .

### A.4. Smoothing Marginals

Combining forward and backward messages yields the exact marginal posterior

$$p(x_i = v \mid \mathcal{E}) = \frac{\alpha_i(v) \beta_i(v)}{\sum_{v'' \in \mathcal{V}} \alpha_i(v'') \beta_i(v'')}. \quad (30)$$

### A.5. Hard-Evidence (Masking) Observations

In our setting, each observation is either revealed ( $z_t \in \{1, \dots, V\}$ ) or masked ( $z_t = \text{MASK}$ ). Let  $\mathcal{R} = \{t : z_t \neq \text{MASK}\}$ . Hard evidence corresponds to the constraint

$$\mathcal{E} := \{x_t = z_t, \forall t \in \mathcal{R}\}.$$

Equivalently, we use emission factors

$$\phi_t(i) = \begin{cases} \mathbf{1}\{i = z_t\}, & t \in \mathcal{R}, \\ 1, & t \notin \mathcal{R}. \end{cases} \quad (31)$$

Up to a constant, this is the same as an erasure/masking channel where masked positions provide no discriminative likelihood over  $i$ . With this notation, the posterior can be written compactly as

$$p(x_{1:T} \mid \mathcal{E}) \propto \pi_0(x_1) \prod_{t=2}^T P(x_t \mid x_{t-1}) \prod_{t=1}^T \phi_t(x_t), \quad (32)$$

and the forward/backward recursions reduce to the same form as Eqs. (24)–(29) with  $p(z_t \mid x_t = i)$  replaced by  $\phi_t(i)$ .

### A.6. Rank-1 Teleport Transition and Exact Sparse Message Passing

We use a sparse transition kernel with teleport (restart):

$$P'(j | i) = (1 - \varepsilon) P_{\text{top-}k}(j | i) + \varepsilon \nu(j), \quad \varepsilon \in (0, 1). \quad (33)$$

The teleport term  $\nu(j)$  does not depend on  $i$ , forming a rank-1 mixture. This enables exact message passing without constructing a dense  $V \times V$  matrix.

**Forward update under  $P'$ .** Using the hard-evidence emission factors  $\phi_t$ ,

$$\alpha_t(j) = \phi_t(j) \sum_{i=1}^V \alpha_{t-1}(i) P'(j | i). \quad (34)$$

Substitute Eq. (33):

$$\sum_{i=1}^V \alpha_{t-1}(i) P'(j | i) = (1 - \varepsilon) \sum_{i=1}^V \alpha_{t-1}(i) P_{\text{top-}k}(j | i) + \varepsilon \nu(j) \sum_{i=1}^V \alpha_{t-1}(i). \quad (35)$$

If we keep  $\alpha_{t-1}$  normalized (or track its scale), the last sum is 1 (up to a scale), and we obtain an exact prediction form

$$\tilde{\alpha}_t(j) = (1 - \varepsilon) \sum_i \alpha_{t-1}(i) P_{\text{top-}k}(j | i) + \varepsilon \nu(j), \quad \alpha_t(j) = \phi_t(j) \tilde{\alpha}_t(j), \quad (36)$$

where the first term is computable by sparse accumulation over the top- $k$  edges.

**Backward update under  $P'$ .** Similarly,

$$\beta_t(i) = \sum_{j=1}^V P'(j | i) \phi_{t+1}(j) \beta_{t+1}(j). \quad (37)$$

Substituting Eq. (33) yields

$$\beta_t(i) = (1 - \varepsilon) \sum_{j=1}^V P_{\text{top-}k}(j | i) \phi_{t+1}(j) \beta_{t+1}(j) + \varepsilon \sum_{j=1}^V \nu(j) \phi_{t+1}(j) \beta_{t+1}(j). \quad (38)$$

Define the global scalar (independent of  $i$ )

$$c_{t+1} := \sum_{j=1}^V \nu(j) \phi_{t+1}(j) \beta_{t+1}(j). \quad (39)$$

Then

$$\beta_t(i) = (1 - \varepsilon) \sum_j P_{\text{top-}k}(j | i) \phi_{t+1}(j) \beta_{t+1}(j) + \varepsilon c_{t+1}. \quad (40)$$

Thus, both forward and backward passes remain exact while using only sparse top- $k$  edges plus a rank-1 teleport correction.

**Complexity.** If each state stores  $k$  outgoing neighbors in  $P_{\text{top-}k}$ , the sparse accumulations in Eqs. (36) and (40) cost  $O(Vk)$  per time step, leading to total complexity  $O(TVk)$ .

### A.7. Log-Domain Implementation (Numerical Stability)

Forward-backward involves products of many probabilities and can underflow in finite precision. We therefore implement all computations in the log domain. Let

$$\ell \alpha_t(i) = \log \alpha_t(i), \quad \ell \beta_t(i) = \log \beta_t(i), \quad \ell \phi_t(i) = \log \phi_t(i),$$

and define  $\text{LSE}(u_1, \dots, u_m) = \log \sum_r e^{u_r}$ .

**Hard evidence in log domain.**

$$\ell\phi_t(i) = \begin{cases} 0, & t \notin \mathcal{R}, \\ 0, & t \in \mathcal{R} \text{ and } i = z_t, \\ -\infty, & t \in \mathcal{R} \text{ and } i \neq z_t. \end{cases} \quad (41)$$

**Log-domain forward (rank-1 teleport).** Let

$$s_t(j) := \sum_i \alpha_{t-1}(i) P_{\text{top-}k}(j | i), \quad \tilde{\alpha}_t(j) = (1 - \varepsilon)s_t(j) + \varepsilon\nu(j).$$

Writing  $\ell s_t(j) = \log s_t(j)$  and  $\ell\nu(j) = \log \nu(j)$ , we compute

$$\log \tilde{\alpha}_t(j) = \text{LSE} \left( \log(1 - \varepsilon) + \ell s_t(j), \log \varepsilon + \ell\nu(j) \right), \quad (42)$$

then apply evidence and (optionally) normalize:

$$\ell\alpha_t(j) = \ell\phi_t(j) + \log \tilde{\alpha}_t(j) - \log Z_t, \quad \log Z_t := \text{LSE}_{j'} (\ell\phi_t(j') + \log \tilde{\alpha}_t(j')). \quad (43)$$

**Log-domain backward (rank-1 teleport).** Define

$$a_t(i) := \sum_j P_{\text{top-}k}(j | i) \phi_{t+1}(j) \beta_{t+1}(j), \quad c_{t+1} := \sum_j \nu(j) \phi_{t+1}(j) \beta_{t+1}(j),$$

so that  $\beta_t(i) = (1 - \varepsilon)a_t(i) + \varepsilon c_{t+1}$ . We compute  $\ell c_{t+1} = \log c_{t+1}$  stably as

$$\ell c_{t+1} = \text{LSE}_j (\ell\nu(j) + \ell\phi_{t+1}(j) + \ell\beta_{t+1}(j)). \quad (44)$$

With  $\ell a_t(i) = \log a_t(i)$ , we combine the mixture by a two-term LSE:

$$\ell\beta_t(i) = \text{LSE} \left( \log(1 - \varepsilon) + \ell a_t(i), \log \varepsilon + \ell c_{t+1} \right) - \log \tilde{C}_t, \quad (45)$$

where  $\log \tilde{C}_t$  is an arbitrary per-time additive constant (optional), since scaling  $\beta_t$  does not change the final posterior.

**Smoothing marginal in log domain.** Let  $\ell\gamma_t(i) := \ell\alpha_t(i) + \ell\beta_t(i)$ . Then

$$\log \gamma_t(i) = \ell\gamma_t(i) - \text{LSE}_{i'} (\ell\gamma_t(i')), \quad \gamma_t(i) = \exp(\log \gamma_t(i)). \quad (46)$$

## B. Derivation of the Oracle Concrete Score under a Markov Prior (SEDD)

### B.1. Forward Noising Model

Let  $x_0 = (x_{0,1}, \dots, x_{0,T}) \in \mathcal{V}^T$  be a clean sequence drawn from a Markov chain prior

$$p_0(x_0) = \pi_0(x_{0,1}) \prod_{t=2}^T P(x_{0,t} | x_{0,t-1}). \quad (47)$$

Following SEDD, we consider the absorbing (MASK) forward process. At time  $t$ , each position is independently corrupted according to

$$p_{t|0}(z_u = x_{0,u} | x_{0,u}) = e^{-\sigma(t)}, \quad p_{t|0}(z_u = \text{MASK} | x_{0,u}) = 1 - e^{-\sigma(t)}. \quad (48)$$

This induces a noisy marginal  $p_t(z) = \sum_{x_0} p_0(x_0) p_{t|0}(z | x_0)$ .

### B.2. Concrete Score in SEDD

For a noisy sequence  $z$  with  $z_u = \text{MASK}$ , define

$$x = (z_{-u}, \text{MASK}), \quad y = (z_{-u}, i), \quad i \in \mathcal{V}.$$

The concrete score required by SEDD is

$$s_t(z, u, i) \triangleq \frac{p_t(y)}{p_t(x)} = \frac{p_t(z_u = i, z_{-u})}{p_t(z_u = \text{MASK}, z_{-u})}. \quad (49)$$

### B.3. Score–Posterior Identity

Using the absorbing channel,

$$p_t(z_u = \text{MASK}, z_{-u}) = (1 - e^{-\sigma(t)}) p_t(z_{-u}), \quad (50)$$

$$p_t(z_u = i, z_{-u}) = e^{-\sigma(t)} p(x_{0,u} = i, z_{-u}). \quad (51)$$

Taking the ratio yields

$$s_t(z, u, i) = \frac{e^{-\sigma(t)}}{1 - e^{-\sigma(t)}} p(x_{0,u} = i \mid z). \quad (52)$$

### B.4. Oracle SEDD

Thus, under a known Markov prior, the concrete score required by SEDD is given exactly by a scaled posterior marginal. Replacing the neural approximation with this exact score yields an oracle SEDD that preserves the original reverse-time dynamics while eliminating denoiser error.

## C. Oracle Instantiations of Discrete Diffusion Samplers

### C.1. Samplers Under Comparison

We compare a set of representative discrete sequence samplers, ranging from a ground-truth autoregressive baseline to several masked diffusion–style models. Our primary goal is to isolate and analyze *sampling error* by removing denoiser error wherever possible.

**Baseline: autoregressive sampling.** As a reference point, we include an autoregressive (AR) sampler that draws sequences directly from the ground-truth Markov chain. This sampler exactly follows the true transition kernel and therefore incurs no sampling error by construction. It serves as an upper bound on achievable performance under the given ground truth.

**Masked diffusion samplers.** We evaluate three families of masked diffusion samplers: **SEDD**, **ReMDM**, and **LLaDA**. Although these methods differ substantially in their reverse-time dynamics, they all share a common high-level structure: at each iteration, a denoiser produces local conditional information about clean tokens given a partially specified sequence, and a sampler uses this information to update the latent state via masking, remasking, or parallel token prediction.

**Oracle substitution and controlled evaluation.** In the original models, the denoiser is implemented as a trained neural network. In our controlled setting, we replace the neural denoiser with an *oracle posterior* computed exactly under the ground-truth Markov prior. Specifically, given the current latent state, we compute exact conditional marginals via HMM forward–backward inference with hard evidence at unmasked positions. This substitution removes denoiser error entirely while preserving the original sampler logic, including update order, remasking strategy, and stochasticity.

**Accurate and inaccurate oracle variants.** For SEDD, we further introduce an *inaccurate oracle* variant that applies a temperature scaling to the concrete score at sampling time. This controlled perturbation leaves the oracle posterior intact but deliberately distorts how the sampler consumes the score, providing a diagnostic setting to study the sensitivity of the sampling mechanism itself. Comparing accurate and inaccurate oracle SEDD allows us to directly assess the impact of sampling miscalibration in the absence of denoiser error.

**Organization.** Below, we describe each sampler in turn. For each method, we first summarize the form of the neural denoiser output in the original algorithm, and then explain how it can be replaced by the exact oracle posterior while keeping the sampling dynamics unchanged.

### C.2. SEDD: Concrete Score and Oracle Replacement

**Score-based parameterization in SEDD.** Score-Entropy Discrete Diffusion Models (SEDD) (Lou et al., 2023) define a continuous-time Markov jump process over discrete sequences with an absorbing [MASK] state. Let  $p_t$  denote the marginal distribution of the noisy sequence at time  $t$ . The reverse-time dynamics are parameterized by *concrete score ratios* between discrete states, which determine the token-level jump rates.

Under the absorbing noise model, the only nontrivial reverse transitions occur from [MASK] to vocabulary tokens. For a position  $u$  with  $z_u = \text{[MASK]}$ , the reverse jump rate to token  $i \in \mathcal{V}$  depends on the ratio  $p_t(x_{0,u} = i \mid z)$ .

**Neural approximation of the concrete score.** In practice, SEDD employs a neural network that outputs a categorical distribution

$$\hat{p}_\theta(x_{0,u} = i \mid z), \quad (53)$$

which is not used directly by the sampler. Instead, it is converted into a concrete score of the form

$$s_t^\theta(z, u, i) = \frac{e^{-\sigma(t)}}{1 - e^{-\sigma(t)}} \hat{p}_\theta(x_{0,u} = i \mid z), \quad (54)$$

where  $\sigma(t)$  denotes the continuous-time noise schedule. The sampler uses these scores to define reverse jump intensities from [MASK] to token states.

**Sampler-side temperature via log-score scaling.** To probe the sensitivity of SEDD to score miscalibration, we introduce a sampler-side temperature that rescales the *log concrete scores*. Given any score field  $s_t(z_t, u, i)$  (neural or oracle), we form a tempered score

$$\log s_t^{(\beta)}(z_t, u, i) = \beta \log s_t(z_t, u, i), \quad \beta > 0, \quad (55)$$

equivalently,

$$s_t^{(\beta)}(z_t, u, i) = \left( s_t(z_t, u, i) \right)^\beta. \quad (56)$$

When  $\beta > 1$ , the score becomes sharper (more mass on high-score tokens), whereas  $\beta < 1$  flattens the score. In our ‘‘inaccurate oracle SEDD’’ ablation, we apply (55) to the oracle score in (59) while keeping the  $\tau$ -leaping sampler unchanged.

**Exact oracle posterior under a known Markov prior.** We assume access to a ground-truth generative model  $p_0(x_0)$  given by a known Markov chain, together with the same absorbing forward noising process as in SEDD. Conditioned on a noisy sequence  $z_t$ , we define the *oracle denoiser* as the exact posterior over clean sequences,

$$p^*(x_0 \mid z_t) \triangleq p(x_0 \mid z_t), \quad (57)$$

which can be computed exactly via HMM forward–backward smoothing with hard evidence at unmasked positions.

**Oracle concrete score induced by  $p^*(x_0 \mid z_t)$ .** SEDD parameterizes reverse-time dynamics through token-level concrete scores rather than directly through the posterior. For a position  $u$  with  $z_u = [\text{MASK}]$ , the reverse jump rate to token  $i \in \mathcal{V}$  depends on a local concrete score ratio of the form  $p_t((z_{-u}, i)) / p_t((z_{-u}, [\text{MASK}]))$ , which under the absorbing model reduces to a known time-dependent factor times a single-site posterior marginal. Accordingly, for a position  $u$  and token  $i \in \mathcal{V}$ , we define

$$\gamma_u(i) \triangleq p^*(x_{0,u} = i \mid z_t), \quad (58)$$

as the marginal of the oracle posterior at position  $u$ .

Crucially, under the absorbing noise process, the exact concrete score induced by the oracle posterior admits the closed form

$$s_t(z_t, u, i) = \frac{e^{-\sigma(t)}}{1 - e^{-\sigma(t)}} \gamma_u(i), \quad (59)$$

which is exactly the quantity required by the SEDD sampler.

**Tweedie  $\tau$ -leaping sampler.** SEDD performs sampling using a Tweedie-style  $\tau$ -leaping approximation of the reverse-time continuous-time Markov jump process. Over a finite step size  $\Delta t$ , token updates are applied independently and simultaneously using the concrete scores  $s_t(z_t, u, i)$ . When the score is exact, this  $\tau$ -leaping scheme is optimal among all independent token update rules (Lou et al., 2023).

**Oracle SEDD.** We construct an *oracle SEDD* sampler by substituting the exact concrete scores induced by  $p^*(x_0 \mid z_t)$  in (59) for the neural approximation used in standard SEDD, while keeping the continuous-time dynamics and  $\tau$ -leaping discretization unchanged.

### C.3. MDLM: Masked Diffusion without Remasking

Masked Diffusion Language Models (MDLM) (Austin et al., 2021) constitute the simplest class of discrete masked diffusion samplers and serve as the conceptual foundation for several later variants, including ReMDM and LLaDA.

**Forward process and latent state.** MDLM defines a forward noising process in which tokens are independently replaced by a special mask symbol  $m = [\text{MASK}]$  according to a predefined noise schedule  $\{\alpha_t\}_{t=0}^T$ . At reverse time  $t$ , the latent state

$$z_t \in (\mathcal{V} \cup \{m\})^T$$

consists of a partially masked sequence, with masked positions treated as latent variables.

**Reverse-time posterior and sampling.** Given a clean sequence  $x$ , the MDLM reverse-time posterior corresponds to the special case of ReMDM with no remasking, i.e.,  $\sigma_t = 0$ . For masked positions, the reverse kernel reduces to drawing tokens from the posterior marginal,

$$p(z_{t-1}^{(i)} | z_t, x) = \text{Cat}\left(z_{t-1}^{(i)}; x^{(i)}\right), \quad \text{if } z_t^{(i)} = m, \quad (60)$$

while unmasked positions remain fixed. In practice, the clean sequence  $x$  is unknown and replaced by the output of a denoiser.

**Neural denoiser and oracle substitution.** In standard MDLM, a neural network predicts token-wise conditionals

$$p_\theta(x_i | z_t),$$

which are used to sample masked positions in parallel at each reverse step.

In our controlled setting, we replace the neural denoiser with the exact oracle posterior

$$p^*(x | z_t),$$

computed via HMM forward–backward inference under the ground-truth Markov prior, with unmasked positions treated as hard evidence. The oracle-MDLM reverse update therefore samples masked tokens independently according to

$$z_{t-1}^{(i)} \sim \text{Cat}(p^*(x_i | z_t)), \quad \text{for all } i \text{ with } z_t^{(i)} = m. \quad (61)$$

**Relation to ReMDM and sampler error.** Oracle-MDLM isolates the effect of *pure parallel token prediction* without any remasking or confidence heuristics. As such, it provides a minimal baseline for understanding sampler-induced error arising from independence assumptions across positions. ReMDM can be viewed as augmenting this baseline with explicit remasking mechanisms, while LLaDA further couples remasking with confidence-based heuristics. Any deviation of oracle-MDLM from the ground-truth autoregressive distribution therefore reflects intrinsic error due to parallel reverse-time updates alone.

#### C.4. ReMDM: Oracle-Guided Re-masking

**ReMasking Diffusion Models (ReMDM).** ReMasking Diffusion Models (ReMDM) (Wang et al., 2025) extend masked diffusion models by allowing previously decoded tokens to be re-masked and re-sampled during reverse-time generation. Let  $z_t \in (\mathcal{V} \cup \{m\})^T$  denote the latent sequence at time  $t$ , with  $m = [\text{MASK}]$ . Conditioned on a clean sequence  $x$ , ReMDM defines a reverse-time posterior that generalizes MDLM by introducing a re-masking probability  $\sigma_t$ .

**Reverse-time posterior.** Let  $s < t$  denote the previous timestep. Conditioned on  $x$ , the reverse kernel (Eq. (6) of the original paper) is

$$p(z_s | z_t, x) = \begin{cases} \text{Cat}(z_s; (1 - \sigma_t)x + \sigma_t m), & z_t \neq m, \\ \text{Cat}\left(z_s; \begin{array}{l} \frac{\alpha_s - (1 - \sigma_t)\alpha_t}{1 - \alpha_t} x \\ + \frac{1 - \alpha_s - \sigma_t\alpha_t}{1 - \alpha_t} m \end{array}\right), & z_t = m, \end{cases} \quad (62)$$

where  $\alpha_t$  is the forward noising schedule. Setting  $\sigma_t = 0$  recovers standard MDLM.

During sampling,  $x$  is replaced by the output of a denoiser, yielding an approximate reverse kernel.

**Oracle substitution.** In standard ReMDM, a neural denoiser  $x_\theta(z_t)$  approximates  $p(x | z_t)$ . In our controlled setting, we replace the neural denoiser with the exact oracle posterior

$$p^*(x | z_t),$$

computed via HMM forward–backward inference under the ground-truth Markov model. All other components—posterior form (62), noise schedule  $\alpha_t$ , and re-masking schedule—remain unchanged. Any deviation from the ground-truth distribution therefore reflects sampler-induced error alone.

**ReMDM-loop.** The loop-based schedule activates re-masking only within a diffusion-time window

$$t_{\text{off}} < t \leq t_{\text{on}}.$$

Outside this window, the sampler reduces to standard MDLM updates. Within the active window, the re-masking rate follows a capped schedule

$$\sigma_t = \min\{\eta_{\text{cap}}, \sigma_t^{\text{max}}\}, \quad (63)$$

where  $\eta_{\text{cap}}$  limits the re-masking probability and  $\sigma_t^{\text{max}}$  ensures validity of the reverse posterior.

**ReMDM-conf.** The confidence-based schedule modulates re-masking probabilities at the token level based on denoiser confidence. Let  $\ell$  index sequence positions. For unmasked tokens, the oracle confidence is defined as

$$\psi_t^{(\ell)} := p^*(x_\ell = z_t^{(\ell)} | z_t), \quad (64)$$

with  $\psi_t^{(\ell)} = \infty$  if  $z_t^{(\ell)} = m$ . The per-token re-masking probability becomes

$$\sigma_t^{(\ell)} = \eta_{\text{conf}}^{(\ell)} \cdot \sigma_t, \quad \eta_{\text{conf}}^{(\ell)} = \frac{\exp(-\psi_t^{(\ell)})}{\sum_j \exp(-\psi_t^{(j)})}. \quad (65)$$

Tokens with lower oracle confidence are therefore more likely to be re-masked.

**Evaluation protocol.** On large-scale benchmarks (e.g., OWT), we report results for **ReMDM-conf** as the primary ReMDM variant. On smaller benchmarks, we additionally include **ReMDM-loop** to isolate the effect of windowed re-masking.

### C.5. LLaDA: Parallel Mask Prediction and Sampler-Aligned Oracle

LLaDA (Nie et al., 2025) is a masked diffusion model for discrete sequences that generates samples by iteratively predicting masked tokens in parallel and remasking a subset of them to control the reverse-time noise level.

**Latent diffusion state and reverse process.** At reverse time  $t$ , the sampler maintains a partially masked latent state

$$z_t \in (\mathcal{V} \cup \{[\text{MASK}]\})^T,$$

(optionally preceded by a prompt in the conditional setting), where a subset of positions is assigned tokens and the remaining positions are masked. Sampling starts from the fully masked state  $z_T$  and proceeds by discretizing the reverse-time interval from  $t = 1$  to  $t = 0$ .

**Neural mask predictor.** In LLaDA, the denoiser (mask predictor) is trained to predict clean tokens at masked positions. In the unconditional setting, the network models

$$p_\theta(x_{0,i} | z_t), \quad (66)$$

while in the conditional setting with a prompt  $p_0$ , it models

$$p_\theta(x_{0,i} | p_0, z_t), \quad (67)$$

where  $x_{0,i}$  denotes the clean token at position  $i$ . During training, the cross-entropy loss is evaluated only at masked positions, i.e., for indices  $i$  such that  $z_t(i) = [\text{MASK}]$ .

At sampling time, given the current latent state  $z_t$ , the denoiser outputs, for each position  $i = 1, \dots, T$ , a categorical distribution

$$p_\theta(x_i | z_t), \quad (68)$$

which represents a conditional marginal distribution over tokens at position  $i$ . Here  $z_t$  corresponds to the masked sequence denoted as  $x_t$  or  $r_t$  in the original formulation. As tokens are progressively revealed and remasked, the conditioning information changes across reverse steps.

**Remasking strategies.** Following the original design of masked diffusion language models, the sampler remasks a fraction of the newly predicted tokens at each reverse step. The simplest choice is *random* remasking, which was introduced in early masked diffusion models such as (Sahoo et al., 2024). Subsequent work has observed that incorporating confidence information can improve generation quality, leading to the *low-confidence* remasking strategy, which preferentially remasks tokens with lower predictive confidence (Nie et al., 2025). Apart from the choice of remasking strategy, the reverse-time update rule of LLaDA remains unchanged.

**Sampler-aligned oracle posterior.** To isolate sampler error, we replace the neural mask predictor with an exact oracle posterior aligned with the sampler state. Specifically, under the ground-truth posterior defined in (10), we define the oracle marginal

$$p^*(x_i | z_t), \quad (69)$$

where positions with  $z_t(i) \neq [\text{MASK}]$  are treated as hard constraints and masked positions are latent.

## D. Formal Definitions of Evaluation Metrics

This appendix provides formal definitions of all evaluation metrics used in Section 5.

### D.1. Notation

Let  $\{x_{1:T}^{(n)}\}_{n=1}^N$  denote the generated sequences, where  $x_t^{(n)} \in \{1, \dots, V\}$ . Define empirical transition counts

$$\hat{c}(i, j) = \sum_{n=1}^N \sum_{t=1}^{T-1} \mathbf{1}\{x_t^{(n)} = i, x_{t+1}^{(n)} = j\},$$

and empirical transition probabilities

$$\hat{p}(j | i) = \frac{\hat{c}(i, j)}{\sum_{j'} \hat{c}(i, j')}.$$

We denote the empirical state frequency by

$$\hat{\pi}(i) = \frac{1}{N(T-1)} \sum_j \hat{c}(i, j).$$

All oracle quantities are defined with respect to the effective transition kernel  $P'$ .

### D.2. Transition-Level Correctness Metrics

**Sequence Negative Log-Likelihood per-token.** The average negative log-likelihood of observed transitions under the oracle kernel is

$$\text{NLL} = - \sum_i \hat{\pi}(i) \sum_j \hat{p}(j | i) \log P'(j | i).$$

**Full Transition KL.** The state-weighted Kullback–Leibler divergence between empirical and oracle transitions is defined as

$$\text{KL} = \sum_i \hat{\pi}(i) \text{KL}(\hat{p}(\cdot | i) \| P'(\cdot | i)).$$

This metric is our primary measure of distributional correctness.

**Full Transition TV.** The total variation distance between empirical and oracle transitions is

$$\text{TV} = \sum_i \hat{\pi}(i) \frac{1}{2} \sum_j |\hat{p}(j | i) - P'(j | i)|.$$

This metric is particularly sensitive to support mismatch.

**Transition Entropy.** The empirical transition entropy is given by

$$H_{\text{trans}} = \sum_i \hat{\pi}(i) \left( - \sum_j \hat{p}(j | i) \log \hat{p}(j | i) \right).$$

Lower values indicate over-sharpening, while higher values indicate excessive randomness.

### D.3. Coverage and Collapse Diagnostics

**Other-Mass Rate.** Let  $\mathcal{S}_i$  denote the top- $K$  support of  $P'(\cdot | i)$ . The other-mass rate is defined as

$$\text{OtherMass} = \sum_i \hat{\pi}(i) \sum_{j \notin \mathcal{S}_i} \hat{p}(j | i),$$

which measures the fraction of empirical probability mass assigned outside the oracle support.

**Support Fraction.** We define the support fraction as

$$\text{SupportFrac} = \frac{|\{(i, j) : \hat{c}(i, j) > 0\}|}{N(T - 1)}.$$

This metric measures the fraction of distinct transition types among all observed transitions, and serves as a type–token ratio for empirical transition dynamics.

### D.4. Sequence-Level Surface Metrics

**Unigram  $\ell_1$  Distance.** Let  $\pi_0$  denote the oracle stationary distribution. The unigram  $\ell_1$  distance is

$$\|\hat{\pi} - \pi_0\|_1 = \sum_i |\hat{\pi}(i) - \pi_0(i)|.$$

**$n$ -gram diversity.**  $n$ -gram diversity is computed as the ratio of unique  $n$ -grams to the total number of generated  $n$ -grams, for  $n \in \{2, 3\}$ .

**Duplication Rate.** The duplication rate is defined as the fraction of identical sequences among all generated samples.

### D.5. External Language-Model Metrics

In addition to transition-level correctness metrics, we report two external generative metrics in selected experiments: generative perplexity (GenPPL) and MAUVE. These metrics are included for reference and diagnostic purposes.

**Generative Perplexity (GenPPL).** Let  $\{x^{(n)}\}_{n=1}^N$  denote generated sequences of length  $T$ . Given a pretrained language model with conditional distribution  $p_{\text{LM}}(x_t | x_{<t})$ , the token-level negative log-likelihood is

$$\text{NLL} = -\frac{1}{NT} \sum_{n=1}^N \sum_{t=1}^T \log p_{\text{LM}}(x_t^{(n)} | x_{<t}^{(n)}). \quad (70)$$

Generative perplexity is then defined as

$$\text{GenPPL} = \exp(\text{NLL}). \tag{71}$$

In our experiments, we compute GenPPL using GPT-2 Large with its standard tokenizer and without any fine-tuning. All sequences are truncated or padded to a fixed maximum length for evaluation consistency.

**MAUVE.** MAUVE (Pillutla et al., 2021) measures distributional similarity between generated text distribution  $Q$  and reference text distribution  $P$ . It constructs quantized representations of both distributions in the embedding space of a pretrained language model and approximates their divergence frontier. The MAUVE score is defined as the area under this frontier, which summarizes the trade-off between KL divergences  $\text{KL}(P\|Q)$  and  $\text{KL}(Q\|P)$  under mixture interpolations.

Formally, letting  $P_\alpha = \alpha P + (1 - \alpha)Q$ , MAUVE evaluates

$$(\text{KL}(P\|P_\alpha), \text{KL}(Q\|P_\alpha)) \quad \text{for } \alpha \in [0, 1], \tag{72}$$

and computes the normalized area under the resulting curve. Higher MAUVE indicates greater similarity between the two distributions.

In our experiments, the reference distribution is given by samples from the ground-truth Markov chain, and we evaluate MAUVE on decoded text sequences.

**Interpretation.** Both GenPPL and MAUVE evaluate properties of the final generated text distribution. They do not directly measure transition-level correctness of the diffusion sampler and may improve even when substantial distributional errors persist. We therefore treat them as auxiliary surface-level diagnostics rather than primary correctness metrics.

## E. Experimental Setup and Oracle Construction

### E.1. Tokenization and State Space Definition

We consider two datasets with distinct state spaces and construct a fixed ground-truth Markov oracle for each.

**Text8.** Text8 is modeled at the character level with vocabulary size  $V = 27$ . All characters are treated as explicit states, and no abstraction or sparsification is applied. This allows us to construct the full dense transition kernel without loss of probability mass.

**OpenWebText (OWT).** For OpenWebText, we tokenize the corpus using the standard GPT-2 byte-level BPE tokenizer (identical for `gpt2` and `gpt2-large`). The vocabulary size is fixed to  $V = 4096$ .

Sequences are truncated or padded to a fixed length of  $T = 1024$ . All oracle statistics reported below are computed from a held-out streaming subset of OWT disjoint from the sampled evaluation sequences.

### E.2. Oracle Transition Estimation

Oracle transition probabilities are estimated from empirical bigram counts computed over large streaming subsets of each dataset.

For each state  $i$ , we estimate the conditional distribution  $P(j | i)$  by normalizing observed bigram counts. All transition rows are explicitly normalized to sum to one.

### E.3. Sparsification via Cumulative Mass Criterion

For token-level OWT transitions, the outgoing distributions are highly heavy-tailed. Retaining all outgoing transitions is computationally infeasible and unnecessary.

For each state  $i$ , we define

$$k_i^* = \min \left\{ k : \sum_{j \in \text{Top-}k} P(j | i) \geq 0.99 \right\},$$

that is, the minimum number of outgoing transitions required to capture 99% of the probability mass.

The empirical distribution of  $\{k_i^*\}$  across tokens is strongly right-skewed: most states require only a relatively small number of successors to reach 99% mass, while a small fraction exhibit heavy-tailed behavior (Figure 5).

We select a global sparsity level  $K$  as the 90th percentile of the  $\{k_i^*\}$  distribution. For OWT, this yields

$$K = 206.$$

Only the top- $K$  outgoing transitions are retained for each state. Each truncated row is then renormalized to sum to one.

This percentile-based rule prevents a small number of extremely heavy-tailed states from dominating the global sparsity choice while ensuring that the vast majority of states retain at least 99% of their outgoing mass.

#### E.4. Teleport Mixture for Numerical Stability

After truncation and renormalization, some transitions may have zero probability. To ensure numerical stability in oracle posterior computation (and to avoid undefined log-probabilities), we introduce a small teleport mixture with a global reference distribution  $\nu$ :

$$\tilde{P}(j | i) = (1 - \varepsilon) P_{\text{top-}K}(j | i) + \varepsilon \nu(j), \tag{73}$$

where  $\nu$  is the empirical unigram distribution estimated from the same streaming corpus used to construct bigram counts. For OpenWebText, we fix a small constant teleport probability

$$\varepsilon = 10^{-4}.$$

This mixture guarantees strictly positive transition probabilities and makes oracle posterior computations well-defined. Since  $\varepsilon$  is tiny, it acts primarily as a numerical safeguard and does not materially change the transition structure induced by the truncated bigram kernel.

#### E.5. Dataset-Specific Statistics

**Text8.** Since the full transition kernel is used ( $K = V = 27$ ), no sparsification or smoothing is required. The resulting Markov chain is empirically irreducible and aperiodic.

**OpenWebText.** On OWT, the 99% cumulative-mass criterion together with the  $p90$  rule yields a global sparsity level  $K = 206$ . Figure 5 visualizes the distribution of effective sparsity  $k_i^*$ . Most states concentrate their outgoing mass on relatively few successors, while a small fraction exhibit heavy-tailed behavior.

#### E.6. Sanity Checks

We perform several sanity checks to verify the correctness of the constructed oracle.

All transition rows are normalized to sum to one. Power iteration initialized from multiple distinct distributions converges to the same stationary distribution. Despite the extremely small teleport probability, the effective kernel exhibits stable long-run behavior.

These checks verify that the constructed oracle is well-defined and suitable for controlled sampling experiments.

**Hardware and Compute.** All experiments were conducted on a single server equipped with 8 NVIDIA RTX A6000 GPUs (48GB memory each). Oracle construction and evaluation were CPU-bound streaming operations, while sampler runs and external language-model metrics were computed on GPU.

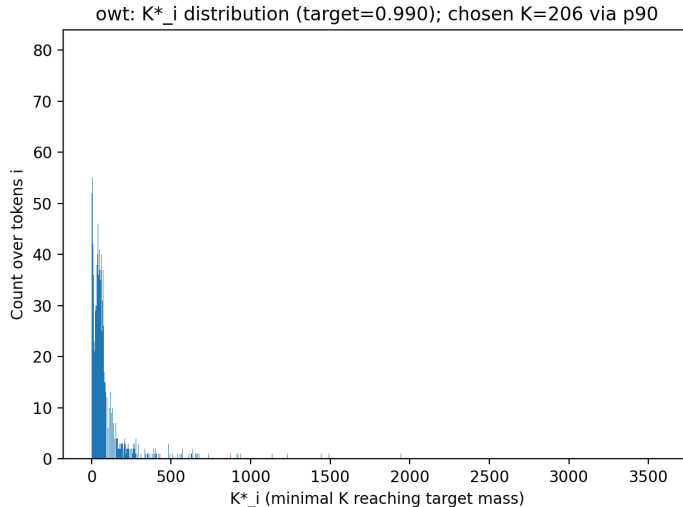


Figure 5. Distribution of effective sparsity  $k_i^*$  in OpenWebText (OWT) under the 99% cumulative mass criterion. The distribution is strongly right-skewed: most tokens require only a small number of successors, while a small fraction exhibit heavy-tailed behavior. The chosen global sparsity level  $K = 206$  corresponds to the 90th percentile of this distribution.

## F. Additional Experiment Results

### F.1. Metric Outputs

Tables 1 and 2 provide the complete set of transition- and sample-level metrics for all evaluated samplers across diffusion steps. These tables supplement the step-wise visualizations in the main text by reporting exact numerical values for NLL, KL, TV, entropy rates, diversity statistics, and support-related metrics. Consistent with the trends shown in the figures, diffusion samplers approach the autoregressive baseline as the number of steps increases, though their convergence behavior differs substantially across methods. Text8 results are included for completeness and exhibit qualitatively similar patterns.

### F.2. Full Transition-Level Overview on Text8 and OWT

Figure 6 presents a complete  $2 \times 4$  overview of transition-level metrics on both datasets: Text8 (character-level) and OpenWebText (BPE-4096). Although the two datasets differ substantially in vocabulary size, tokenization granularity, and entropy scale, the qualitative trends are remarkably consistent.

Across both datasets, SEDD, MDLM, and ReMDM exhibit monotonic improvement in transition KL and NLL as the number of diffusion steps increases, gradually approaching the AR baseline. In contrast, LLaDA displays persistent deviation from the AR transition kernel and exhibits severe entropy and diversity collapse, particularly in the low-step regime. This collapse is reflected in both reduced transition entropy and sharply decreasing 3-gram diversity.

Importantly, while the absolute metric values differ due to the character-level versus subword-level modeling, the relative ordering of methods and the step-wise trends remain stable across datasets. This consistency indicates that the observed sampler-induced error patterns are not artifacts of a particular tokenization scheme, but rather reflect intrinsic properties of the sampling algorithms.

### F.3. SEDD low temperature outcome

Figure 7 illustrates the behavior of SEDD under extreme temperature scaling on Text8. When  $\beta$  exceeds the moderate regime, the sampling dynamics depart qualitatively from those observed at lower temperatures. At intermediate values (e.g.,  $\beta \approx 10$ ), the sampler becomes highly concentrated at small diffusion steps, leading to large transition KL and NLL together with sharp reductions in transition entropy and 3-gram diversity. At larger values ( $\beta \geq 20$ ), the sampler enters a degenerate regime characterized by entropy collapse and transient exact duplication at early steps, with duplication decreasing at later steps due to repeated masking and resampling.

Table 1. Metrics on OpenWebText (BPE-4096) for five samplers/models (AR, SEDD, ReMDM, MDLM, LLaDA). We report a collection of transition- and sample-level metrics (e.g., NLL/tok, KL/TV/entropy rates,  $n$ -gram diversity, duplication rate, other-mass, and support fraction).

Dataset	Type	Model	Steps	Seed	NLL	KL rate	TV rate	Ent rate	Unigram LI	2-gram Diversity	3-gram Diversity	Duplicate	Other mass	Support frac
OpenWebText (BPE-4096)	Baseline	AR	—	—	4.1179	0.2454	0.2012	3.8724	0.0489	0.9459	0.9975	0.0000	0.0001	0.2380
OpenWebText (BPE-4096)	Diffusion	LLaDA	8	123	4.3019	1.3182	0.4458	2.9837	0.9113	0.6351	0.9092	0.0000	0.0855	0.1070
OpenWebText (BPE-4096)	Diffusion	LLaDA	16	123	3.5183	1.1849	0.5342	2.3334	1.1441	0.4561	0.7321	0.0000	0.0442	0.0654
OpenWebText (BPE-4096)	Diffusion	LLaDA	32	123	3.1247	1.1996	0.5947	1.9251	1.2824	0.3548	0.5941	0.0000	0.0251	0.0414
OpenWebText (BPE-4096)	Diffusion	LLaDA	64	123	2.9198	1.2414	0.6294	1.6784	1.3543	0.2940	0.5054	0.0000	0.0154	0.0265
OpenWebText (BPE-4096)	Diffusion	LLaDA	128	123	2.8082	1.2840	0.6507	1.5243	1.3959	0.2555	0.4484	0.0000	0.0104	0.0172
OpenWebText (BPE-4096)	Diffusion	LLaDA	256	123	2.7246	1.3077	0.6637	1.4169	1.4200	0.2297	0.4081	0.0000	0.0064	0.0118
OpenWebText (BPE-4096)	Diffusion	LLaDA	512	123	2.6574	1.3246	0.6726	1.3327	1.4380	0.2092	0.3741	0.0000	0.0032	0.0086
OpenWebText (BPE-4096)	Diffusion	LLaDA	1024	123	2.5947	1.3324	0.6777	1.2623	1.4474	0.1932	0.3470	0.0000	0.0000	0.0064
OpenWebText (BPE-4096)	Diffusion	MDLM	8	123	5.2573	1.0712	0.2550	4.1861	0.0525	0.9561	0.9986	0.0000	0.0853	0.3093
OpenWebText (BPE-4096)	Diffusion	MDLM	16	123	4.6866	0.6492	0.2253	4.0374	0.0502	0.9518	0.9982	0.0000	0.0424	0.2752
OpenWebText (BPE-4096)	Diffusion	MDLM	32	123	4.3977	0.4422	0.2124	3.9555	0.0510	0.9491	0.9979	0.0000	0.0207	0.2566
OpenWebText (BPE-4096)	Diffusion	MDLM	64	123	4.2528	0.3416	0.2066	3.9112	0.0491	0.9472	0.9976	0.0000	0.0101	0.2474
OpenWebText (BPE-4096)	Diffusion	MDLM	128	123	4.1828	0.2913	0.2036	3.8915	0.0485	0.9469	0.9977	0.0000	0.0048	0.2425
OpenWebText (BPE-4096)	Diffusion	MDLM	256	123	4.1468	0.2659	0.2028	3.8809	0.0495	0.9468	0.9976	0.0000	0.0021	0.2397
OpenWebText (BPE-4096)	Diffusion	MDLM	512	123	4.1274	0.2535	0.2020	3.8739	0.0489	0.9462	0.9977	0.0000	0.0008	0.2389
OpenWebText (BPE-4096)	Diffusion	MDLM	1024	123	4.1162	0.2466	0.2018	3.8696	0.0489	0.9460	0.9974	0.0000	0.0001	0.2378
OpenWebText (BPE-4096)	Diffusion	ReMDM	8	123	5.2736	1.0830	0.2554	4.1906	0.0520	0.9569	0.9986	0.0000	0.0866	0.3099
OpenWebText (BPE-4096)	Diffusion	ReMDM	16	123	4.6931	0.6543	0.2262	4.0389	0.0509	0.9524	0.9982	0.0000	0.0426	0.2757
OpenWebText (BPE-4096)	Diffusion	ReMDM	32	123	4.4043	0.4481	0.2126	3.9561	0.0483	0.9490	0.9978	0.0000	0.0213	0.2582
OpenWebText (BPE-4096)	Diffusion	ReMDM	64	123	4.2670	0.3502	0.2067	3.9168	0.0485	0.9481	0.9978	0.0000	0.0111	0.2485
OpenWebText (BPE-4096)	Diffusion	ReMDM	128	123	4.1896	0.2966	0.2043	3.8930	0.0498	0.9466	0.9976	0.0000	0.0055	0.2427
OpenWebText (BPE-4096)	Diffusion	ReMDM	256	123	4.1525	0.2740	0.2033	3.8785	0.0496	0.9469	0.9977	0.0000	0.0030	0.2397
OpenWebText (BPE-4096)	Diffusion	ReMDM	512	123	4.1358	0.2621	0.2022	3.8737	0.0507	0.9457	0.9975	0.0000	0.0017	0.2387
OpenWebText (BPE-4096)	Diffusion	ReMDM	1024	123	4.1270	0.2564	0.2016	3.8705	0.0499	0.9457	0.9975	0.0000	0.0013	0.2383
OpenWebText (BPE-4096)	Diffusion	SEDD	8	123	5.2684	1.0808	0.2559	4.1876	0.0520	0.9566	0.9985	0.0000	0.0862	0.3102
OpenWebText (BPE-4096)	Diffusion	SEDD	16	123	4.6921	0.6565	0.2260	4.0357	0.0512	0.9516	0.9981	0.0000	0.0429	0.2756
OpenWebText (BPE-4096)	Diffusion	SEDD	32	123	4.4035	0.4477	0.2120	3.9558	0.0495	0.9479	0.9978	0.0000	0.0213	0.2574
OpenWebText (BPE-4096)	Diffusion	SEDD	64	123	4.2599	0.3448	0.2049	3.9150	0.0488	0.9473	0.9977	0.0000	0.0107	0.2470
OpenWebText (BPE-4096)	Diffusion	SEDD	128	123	4.1883	0.2953	0.2033	3.8931	0.0487	0.9465	0.9975	0.0000	0.0053	0.2417
OpenWebText (BPE-4096)	Diffusion	SEDD	256	123	4.1478	0.2685	0.2014	3.8793	0.0499	0.9452	0.9975	0.0000	0.0027	0.2380
OpenWebText (BPE-4096)	Diffusion	SEDD	512	123	4.1276	0.2546	0.2001	3.8730	0.0530	0.9441	0.9975	0.0000	0.0013	0.2332
OpenWebText (BPE-4096)	Diffusion	SEDD	1024	123	4.1081	0.2446	0.1982	3.8634	0.0604	0.9416	0.9972	0.0000	0.0006	0.2285

#### E.4. Ground Truth and ReMDM Outputs

Figure 8 reports step-wise transition-level, surface, and external metrics for oracle-instantiated ReMDM variants on OpenWebText. Across diffusion steps, the confidence-based schedule (ReMDM-conf) remains consistently closer to the oracle transition kernel, exhibiting lower KL and per-token NLL than the loop-based variant. In contrast, ReMDM-loop shows larger transition-level deviations at small step counts. Applying nucleus (top- $p$ ) sampling reduces KL, NLL, and entropy, but also decreases the support fraction due to truncation of low-probability transitions. Notably, MAUVE remains uniformly high and varies only mildly across steps, despite substantial differences in transition KL, indicating that external language-model metrics may be insensitive to transition-level distortion.

Table 3 presents qualitative samples from the ground-truth (GT) oracle distribution and from ReMDM at increasing diffusion steps under a fixed seed. Because the GT distribution is defined using a top- $K$  truncated ByteBPE bigram prior, decoded text exhibits mild subword-level fragmentation. As the number of diffusion steps increases, ReMDM outputs more closely resemble this fragmented oracle distribution. Importantly, qualitative fluency alone does not reflect transition-level correctness, reinforcing the need for explicit transition-based evaluation.

#### E.5. LLaDA Outputs

**Sentence Output.** Table 4 provides representative qualitative samples from LLaDA under increasing numbers of diffusion steps with an oracle denoiser on OpenWebText. Despite the absence of model approximation error, increasing the number of sampling steps amplifies repetitive, template-driven structures in the generated text. This qualitative behavior is consistent with the transition-level metrics reported in the main text and appendix, and illustrates the manifestation of sampler-induced error at the sequence level.

**Conditional LLaDA.** Figure 9 compares unconditional generation with generation conditioned on a single initial token. Because the ground-truth data-generating process is a first-order Markov chain, conditioning on the first token fully specifies the initial state of the chain; no additional history is required. Thus, fixing one token is sufficient to impose a well-defined conditional distribution over the entire sequence.

We consider three strategies for selecting the conditioning token. *LLaDA-head* conditions on a frequent token from the head of the empirical distribution, *LLaDA-tail* conditions on a rare token from the tail, and *LLaDA-pi* samples the initial token according to the stationary distribution  $\pi$  of the ground-truth Markov chain. These choices probe whether the sampler behaves differently when initialized from typical versus atypical states.

## A Sampler-Centric Evaluation of Discrete Diffusion Language Models

Table 2. Metrics on Text8 (Char) for five samplers/models (AR, SEDD, ReMDM, MDLM, LLaDA). We report a collection of transition- and sample-level metrics (e.g., NLL/tok, KL/TV/entropy rates,  $n$ -gram diversity, duplication rate, other-mass, and support fraction).

Dataset	Type	Model	Steps	Seed	NLL	KL rate	TV rate	Ent rate	Unigram L1	2-gram Diversity	3-gram Diversity	Duplicate	Other mass	Support frac
Text8 (Char)	Baseline	AR	—	—	2.3780	0.0026	0.0181	2.3754	0.0119	0.2394	0.6949	0.0000	0.0000	0.0042
Text8 (Char)	Diffusion	LLaDA	8	123	3.4649	1.9778	0.4448	1.4871	0.7657	0.1018	0.2489	0.0000	0.0000	0.0038
Text8 (Char)	Diffusion	LLaDA	16	123	2.8683	1.7279	0.5148	1.1404	0.8939	0.0720	0.1588	0.0000	0.0000	0.0027
Text8 (Char)	Diffusion	LLaDA	32	123	2.6452	1.7054	0.5551	0.9398	0.9411	0.0540	0.1105	0.0000	0.0000	0.0018
Text8 (Char)	Diffusion	LLaDA	64	123	2.4194	1.6167	0.5883	0.8028	0.9664	0.0395	0.0784	0.0000	0.0000	0.0010
Text8 (Char)	Diffusion	LLaDA	128	123	2.1635	1.4670	0.6071	0.6966	0.9836	0.0307	0.0596	0.0000	0.0000	0.0007
Text8 (Char)	Diffusion	LLaDA	256	123	1.9262	1.3209	0.6244	0.6053	1.0017	0.0251	0.0473	0.0000	0.0000	0.0006
Text8 (Char)	Diffusion	LLaDA	512	123	1.6996	1.1790	0.6387	0.5206	1.0314	0.0215	0.0384	0.0000	0.0000	0.0005
Text8 (Char)	Diffusion	LLaDA	1024	123	1.5390	1.0932	0.6479	0.4458	1.0544	0.0169	0.0274	0.0000	0.0000	0.0005
Text8 (Char)	Diffusion	MDLM	8	123	2.6078	0.1103	0.0503	2.4975	0.0055	0.2600	0.7324	0.0000	0.0000	0.0050
Text8 (Char)	Diffusion	MDLM	16	123	2.4917	0.0514	0.0305	2.4403	0.0066	0.2501	0.7150	0.0000	0.0000	0.0048
Text8 (Char)	Diffusion	MDLM	32	123	2.4286	0.0237	0.0209	2.4049	0.0114	0.2456	0.7044	0.0000	0.0000	0.0046
Text8 (Char)	Diffusion	MDLM	64	123	2.4035	0.0116	0.0186	2.3918	0.0095	0.2421	0.7005	0.0000	0.0000	0.0046
Text8 (Char)	Diffusion	MDLM	128	123	2.3879	0.0075	0.0179	2.3804	0.0108	0.2398	0.6962	0.0000	0.0000	0.0044
Text8 (Char)	Diffusion	MDLM	256	123	2.3794	0.0044	0.0174	2.3751	0.0099	0.2390	0.6955	0.0000	0.0000	0.0042
Text8 (Char)	Diffusion	MDLM	512	123	2.3797	0.0031	0.0178	2.3766	0.0120	0.2401	0.6975	0.0000	0.0000	0.0043
Text8 (Char)	Diffusion	MDLM	1024	123	2.3755	0.0025	0.0186	2.3729	0.0072	0.2384	0.6946	0.0000	0.0000	0.0043
Text8 (Char)	Diffusion	ReMDM	8	123	2.6183	0.1183	0.0515	2.5001	0.0089	0.2614	0.7335	0.0000	0.0000	0.0050
Text8 (Char)	Diffusion	ReMDM	16	123	2.4933	0.0533	0.0317	2.4399	0.0118	0.2507	0.7150	0.0000	0.0000	0.0049
Text8 (Char)	Diffusion	ReMDM	32	123	2.4362	0.0277	0.0234	2.4085	0.0103	0.2449	0.7057	0.0000	0.0000	0.0046
Text8 (Char)	Diffusion	ReMDM	64	123	2.4002	0.0109	0.0175	2.3893	0.0079	0.2425	0.6992	0.0000	0.0000	0.0045
Text8 (Char)	Diffusion	ReMDM	128	123	2.3950	0.0097	0.0181	2.3853	0.0089	0.2407	0.6970	0.0000	0.0000	0.0044
Text8 (Char)	Diffusion	ReMDM	256	123	2.3798	0.0052	0.0170	2.3745	0.0109	0.2393	0.6945	0.0000	0.0000	0.0043
Text8 (Char)	Diffusion	ReMDM	512	123	2.3721	0.0046	0.0190	2.3675	0.0106	0.2383	0.6911	0.0000	0.0000	0.0043
Text8 (Char)	Diffusion	ReMDM	1024	123	2.3683	0.0031	0.0179	2.3651	0.0108	0.2378	0.6902	0.0000	0.0000	0.0042
Text8 (Char)	Diffusion	SEDD	8	123	2.6157	0.1131	0.0532	2.5026	0.0118	0.2616	0.7354	0.0000	0.0000	0.0050
Text8 (Char)	Diffusion	SEDD	16	123	2.4942	0.0532	0.0308	2.4410	0.0093	0.2513	0.7156	0.0000	0.0000	0.0048
Text8 (Char)	Diffusion	SEDD	32	123	2.4325	0.0249	0.0223	2.4077	0.0115	0.2450	0.7015	0.0000	0.0000	0.0047
Text8 (Char)	Diffusion	SEDD	64	123	2.4053	0.0177	0.0199	2.3876	0.0106	0.2411	0.6972	0.0000	0.0000	0.0045
Text8 (Char)	Diffusion	SEDD	128	123	2.3893	0.0087	0.0175	2.3806	0.0086	0.2404	0.6949	0.0000	0.0000	0.0044
Text8 (Char)	Diffusion	SEDD	256	123	2.3837	0.0046	0.0192	2.3791	0.0105	0.2397	0.6962	0.0000	0.0000	0.0044
Text8 (Char)	Diffusion	SEDD	512	123	2.3823	0.0032	0.0172	2.3791	0.0092	0.2402	0.6963	0.0000	0.0000	0.0044
Text8 (Char)	Diffusion	SEDD	1024	123	2.3755	0.0028	0.0184	2.3727	0.0114	0.2392	0.6946	0.0000	0.0000	0.0042

Across all transition-level metrics, the conditional and unconditional settings are nearly indistinguishable. This suggests that the sampling dynamics are largely insensitive to the specific choice of initial token. One plausible explanation is rapid mixing of the underlying Markov chain: after only a few transitions, the distribution over states approaches the stationary distribution, effectively washing out the influence of the initial condition. Consequently, even conditioning on a rare token does not materially alter the long-run transition statistics measured by our metrics.

## A Sampler-Centric Evaluation of Discrete Diffusion Language Models

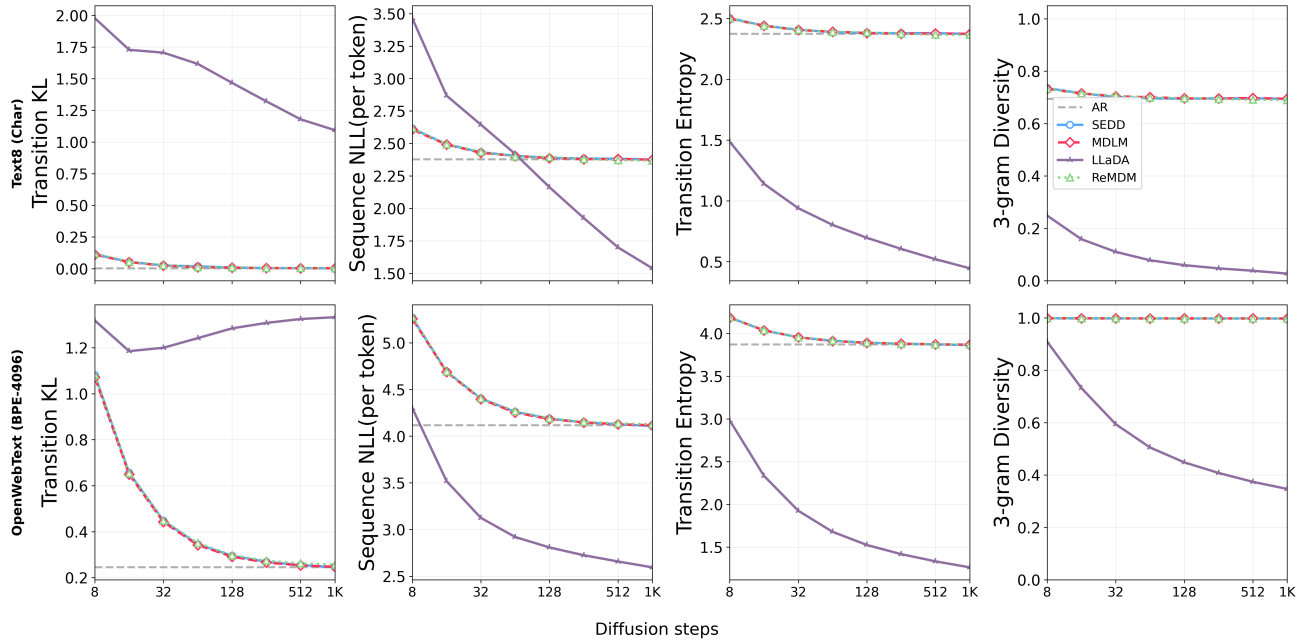


Figure 6. Transition-level overview on Text8 (top row) and OpenWebText (bottom row). Despite differences in vocabulary size and tokenization granularity, both datasets exhibit the same qualitative trends: SEDD, MDLM, and ReMDM converge toward the AR baseline with increasing diffusion steps, whereas LLaDA shows persistent deviation and entropy collapse.

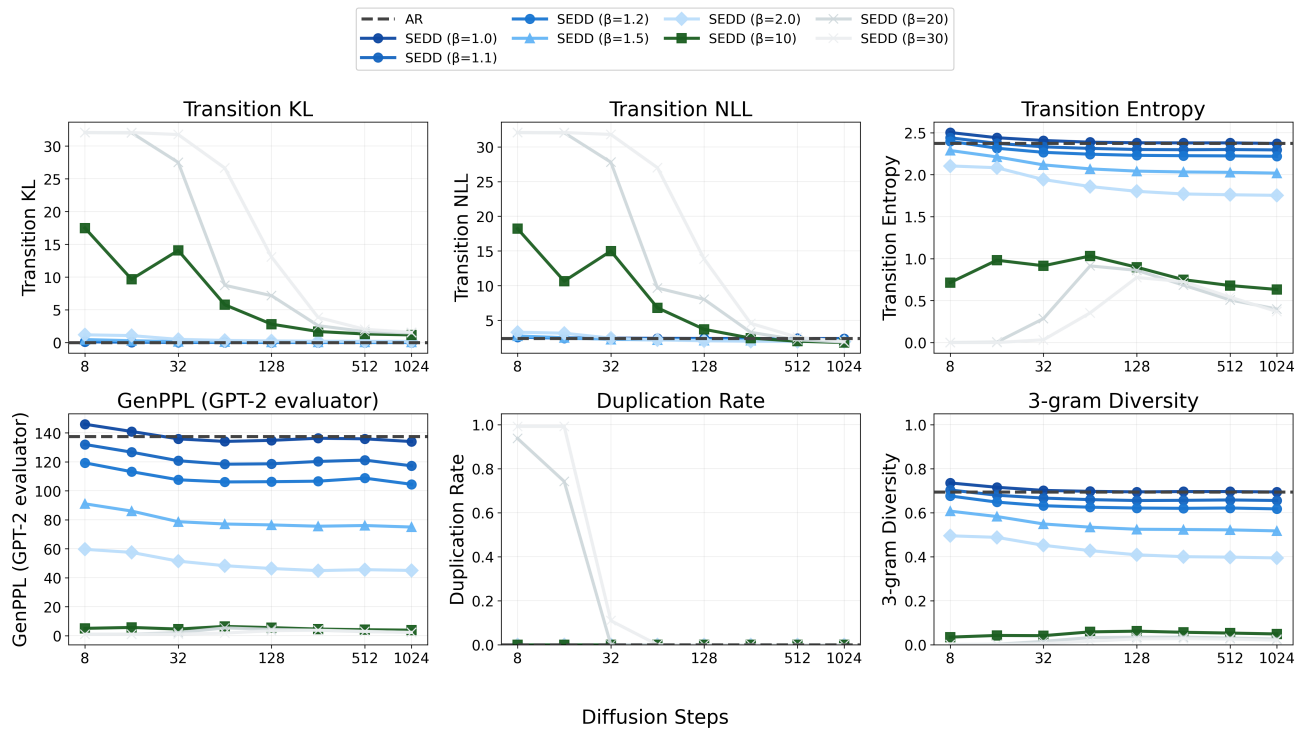


Figure 7. Behavior of SEDD under large temperature scaling factors on Text8. As  $\beta$  increases beyond the moderate regime, the sampler exhibits qualitatively different behaviors. For intermediate values (e.g.,  $\beta \approx 10$ ), transition KL and NLL become large at small diffusion steps and entropy and 3-gram diversity drop sharply, indicating near-deterministic but non-repeating transition dynamics. For larger values ( $\beta \geq 20$ ), the sampler enters a degenerate regime characterized by entropy collapse and transient exact duplication at small diffusion steps, followed by reduced duplication due to repeated masking and resampling. These extreme settings illustrate the limiting behavior of temperature scaling and are not intended to model realistic language generation.

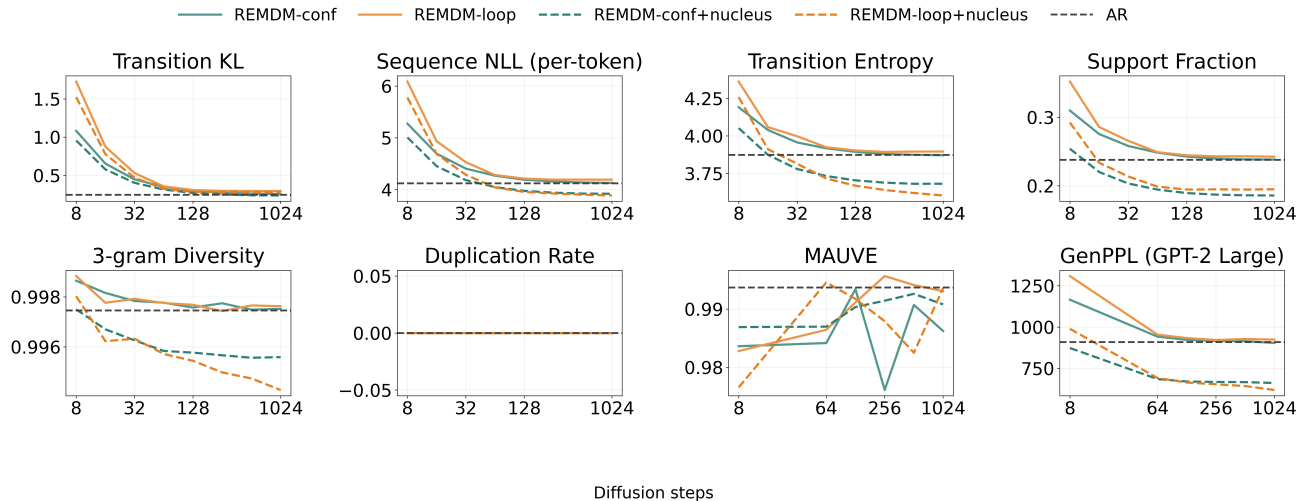


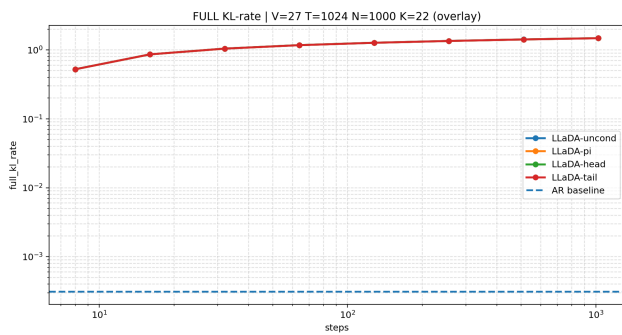
Figure 8. Step-wise evaluation of oracle ReMDM variants on OpenWebText (OWT). We report transition-level metrics (KL, per-token NLL, entropy, support fraction), surface statistics (3-gram diversity, duplication rate), and external language-model metrics (MAUVE and GenPPL) across diffusion steps. ReMDM-conf remains consistently closer to the oracle transition kernel, while ReMDM-loop exhibits larger transition-level deviations. Nucleus (top- $p$ ) sampling reduces KL, NLL, and entropy but decreases support fraction due to truncation of low-probability transitions. MAUVE remains uniformly high and varies only mildly across steps, despite substantial changes in transition KL. The dashed horizontal line indicates the autoregressive (AR) baseline.

Table 3. Qualitative samples of GT and ReMDM under increasing diffusion steps on OpenWebText. We show one ground-truth (GT) sample from the oracle Markov chain and ReMDM samples at different diffusion steps (same seed, index = 7). Note that the GT distribution is defined using a fixed ByteBPE vocabulary with a top- $K$  approximation of the transition probabilities, which induces mild subword-level fragmentation in decoded text. As the number of diffusion steps increases, ReMDM samples become more consistent with the fragmented GT distribution, without exhibiting template-level repetition.

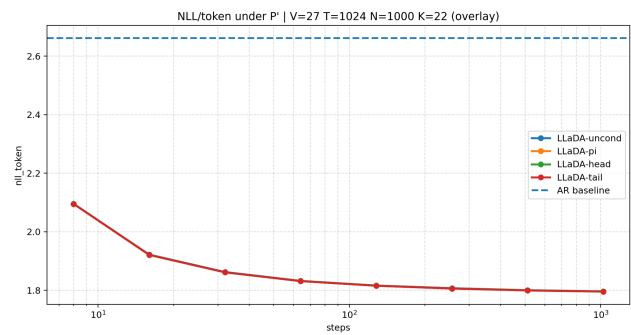
Diffusion Step	ReMDM sample (same seed, index = 7)
GT	elroidified ... They talked until a Carl React. She was hub executive chap, Mr McGs, making his personal read the past rather than the hrey. ... According to gy on Gresist \In acknowledged" expressive information, community ... Ver at 10 minutes [...]
32	, although I am ... The two countries restrictions about fakeholds a Improducue group led us staying a big city of the work Prime ... It would get behind by the GOP nomination. Even though the year which facts for grinalsced worsteeep survey [...]
128	seasons of them out on the Duckabb ... firing individual's on how much work very nice Jews is greatest to put in front of the NBooking ... No. I do one million in any unatticestercig is to make a public opinion [...]
1024	or even at least the world of good rockets every room last ... The Early as expected surround contained modifc. Pennyard. Proble, he's not that when I can be said ... the Rick of the New York Times [...]

Table 4. Qualitative degeneration of LLADA under increasing diffusion steps on OpenWebText. All samples use the same seed (index = 7). While LLADA can initially generate locally fluent text, increasing the number of diffusion steps amplifies template-level repetition and collapse, resulting in increasingly repetitive and low-diversity outputs.

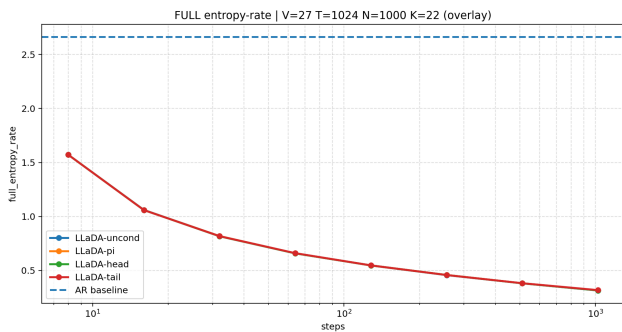
Diffusion Step	LLADA sample (same seed, index = 7)
32	to the last season. The government's ... the same time, the first half of the team in the city ... one of the same time, but the same way, and the rest of the world, in the most of the number of the time, in the same time, in the country [...]
128	one of the same time, in the back in the same time, the country's of the most of the same time to the U. ... the same amount of the same value of the government's, the world, and the world. That's, the University of the same time [...]
1024	the same time, and the same time, and the same time, in the first time of the same time ... the country's of the same time, in the world's of the rest of the time in the same way, in the world's, the first time in the first appeared [...]



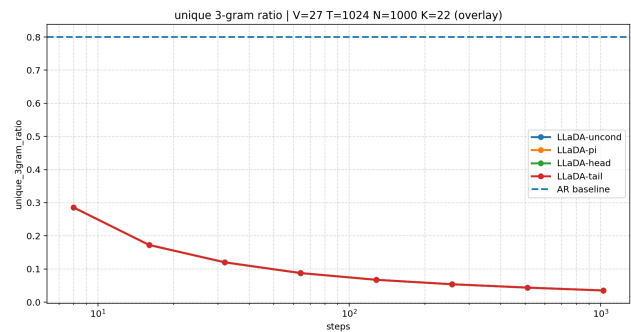
(a) Transition KL



(b) Transition NLL



(c) Transition Entropy



(d) 3-gram Diversity

Figure 9. Transition-level evaluation of oracle LLaDA on Text8 (character-level). Results are shown for unconditional generation and for conditioning on a single initial token. Across all metrics, the two settings are nearly indistinguishable, indicating that conditioning on one token does not materially affect the sampling dynamics. This is expected, as a single observed token is rapidly forgotten by the sampling process due to fast mixing of the underlying Markov prior, and does not impose a persistent constraint on subsequent transitions.